CHARACTERIZATION OF THE CRUSTAL VELOCITY FIELD IN SPACE AND TIME USING AMBIENT SEISMIC NOISE

DISSERTATION

Zur Erlangung des Grades eines

DOKTORS DER NATURWISSENSCHAFTEN

Am Fachbereich Geowissenschaften

der Freien Universität Berlin

vorgelegt von

MSc. Diğdem Acarel

Berlin, December 2014

EHRENWÖRTLICHE ERKLÄRUNG:

Hiermit versichere ich, das ich die vorliegende Dissertation selbständig und nur mit den angegebenen Quellen bzw. Hilfsmitteln angefertigt und verfasst habe.

Berlin, den 11.12.2014

Referent:	Prof. Dr. Marco Bohnhoff
Korreferent:	Prof. Dr. Frederik Tilmann
Datum der Disputation:	20 March 2015

Freie Universität Berlin
Fachbereich Geowissenschaften
Institut für Geologische Wissenchaften
Malteserstr. 74-100
12249 Berlin

SUMMARY

Exploring the interior of the Earth, particularly at seismogenic depths is a long sought goal for seismologists in order to better understand the nucleation and monitoring of devastating earthquakes and better estimate future seismic risks. The success of traditional imaging methods is highly related to how densely the target area is sampled with ray paths between the source and receivers. In case of low seismicity and scarce earthquake-receiver distribution, employing seismic ambient noise, a ubiquitous source, is proved to be an alternative approach. The cross-correlations of seismic ambient noise can be used to estimate the Green' s function of the medium and thus to determine the Earth' s structure.

The main goal of this study is to provide a comprehension on spatial and temporal variation of seismic velocity field at different phases of the seismic cycle. To achieve this, a structural investigation was performed applying seismic ambient noise analysis in the eastern Sea of Marmara region. Another application is in order to monitor potential velocity changes associated with a major earthquake occurred in Van region, eastern Turkey.

In the first part of this thesis, once the necessary pre-processing steps applied to the raw data, ambient noise cross correlation technique is used in order to investigate the crustal structure surrounding the Çınarcık Basin (offshore Istanbul), hosting Princes' Islands segment of the North Anatolian Fault Zone which is in the final phase of the seismic cycle. Low velocity zones of Çınarcık and Thrace Basins in the study area are successfully observed in group velocity dispersion curves, proving ambient noise cross correlation approach to be a feasible and powerful tool for imaging. As a latter step, a 1D S-wave velocity structure is obtained from an average dispersion curve and employed in the inversion process to present the improvement in hypocenter determination.

In the second part, potential variations in the seismic velocity associated with the 2011 M7.1 Van earthquake is investigated by exploting the repeatibility of seismic

ambient noise. Six-month data framing the mainshock is investigated. A coseismic velocity decrease directly related to the Van mainshock is observed in the near vicinity of the earthquake hypocenter. This change in velocity is explained by a coseismic stress change at depth taking into account the frequency band of interest. Moreover, a correlation between the coseismic velocity decrease with minimum distance of the respective ray path to the mainshock hypocenter and the amount of coseismic slip is presented.

ZUSAMMENFASSUNG

Die Erforschung des Erdinnern ist ein seit Jahrzehnten bestehendes zentrales Ziel der instrumentellen Seismologie. Dies betrifft im Besonderen den oberen –seismogenen- Bereich der Erdkruste, der die überwiegende Anzahl starker Erdbeben generiert und damit massgeblich für die seismische Gefährdung und das resultierende seismische Risio verantwortlich ist.

Das Bestreben der Abbildung (imaging) von Strukturen innerhalb der Erdkruste und des Geschwindigkeitsfeldes hat traditionell zwei Ansätze verfolgt: Die Registrierung elastischer Wellen durch Nutzung natürlicher Quellen (Erdbeben) und die gezielte Erkundung entlang von (meistens) 2D-Profilen unter Einsatz künstlicher Energieanregung (Sprengungen, Vibroseis, Airguns). Der erfolgreiche Einsatz beider Methoden hängt von guter Strahlenüberdeckung seismischer Wellen im Untersuchungsgebiet ab und ist damit in großem Umfang gebunden an die (nicht beeinflussbare) räumliche Verteilung von Erdbeben und der limitierten Möglichkeit, die Vermessung aktiver seismischer Profile in besiedelten Gebieten durchzuführen.

In den letzten Jahren hat sich als ein weiteres –drittes- Verfahren die Nutzung und systematische Prozessierung des Hintergrundrauschens (ambient noise) etabliert. Das Hintergrundrauschen ist eine immer und überall verfügbare Signalquelle, die im Wesentlichen durch Wasserbewegungen in den Ozeanen generiert wird.

In der vorliegenden Dissertation wird die systematische Analyse von ‚ambient noise' mit zwei unterschiedlichen Zielen zum Einsazt gebracht: Zur strukturellen Abbildung der oberen etwa 10 Kilometer in der Region des östlichen Marmarameeres und zur Erfassung möglicher zeitlicher Variationen im Geschwindigkeitsfeld der seismogenen Erdkruste im Zuge des Van-Erdbebens in der Osttürkei von 2011, das eine Magnitude von M=7.1 hatte.

In der ersten Teilstudie werden kontinuierliche Messungen von Seismometerstationen rund um das östliche Marmarameer ausgewertet, in der ein Erdbeben mit einer Magnitude bis zu 7.5 in naher Zukunft sehr wahrscheinlich ist. Zwischen den beiden Hauptästen der Nordanatolischen Verwerfungszone unterhalb des Marmarameeres befindet sich ein pull-apart Sedimentbecken (Cinarcik-Becken), dessen Struktur und Tiefenerstreckung hier bestimmt werden soll, um ein detaillierteres tektonisches

Modell der Region zu generieren. Die Bestimmung von 1D-Scherwellen-geschwindigkeits-Tiefen-Modellen erlaubt die Identifikation des Cinarcik-Beckens als Niedergeschwindigkeitsbereich zwischen dem Prinzen-Inseln-Segment im Norden und der Armutlu-Verwerfung im Süden. Auch das wesentlich ältere Thrace-Becken kann durch einen Bereich verringerter Geschwindigkeiten in den Dispersionskurven erkannt und charakterisiert werden. Darüber hinaus dienen die Ergebnisse dieser Studie einem weiteren elementaren Zweck: Durch die erstmalige direkte Bestimmung eine S-Wellen-Geschwindigkeits-Modells für die Region können nun Hypozentren lokaler Seismizität genauer bestimmt werden (vormals musste die S-Wellengeschwindigkeit unter Annahme ideal elastischen Verhaltens aus der P-Geschwindigkeit abgeleitet werden). Die verbesserte Lokalisierungsgenauigkeit wird anhand der Lokalisierung von Steinbruchsprengungen im Raum Istanbul quantifiziert.
In der zweiten Teilstudie werden mögliche zeitliche Variationen im krustalen Geschwindigkeitsfeld im Zusammenhang mit dem 2001 Van-Erdbeben in der Osttürkei untersucht. Dabei werden kontinuierliche ‚ambient-noise'-Registrierungen lokaler Breitbandstationen vor und nach dem Beben über einen Zeitraum von sechs Monaten ausgewertet. Die Ergebnisse zeigen eine klare co-seismisch verursachte Geschwindigkeitsabnahme, die auch eine Frequenzabhängigkeit aufweist. Darüber hinaus weisen die Ergebnisse darauf hin, dass die Geschwindigkeitsabnahme mit der Entfernung (umgekehrt proportional) und der Höhe des co-seismischen Versatzes auf der Bruchfläche (proportional) ist.

CONTENTS

Chapter 1

Introduction: Motivation and outline

Exploring the interior of the Earth is a long sought interest for seismologists in order to better understand the origin and driving mechanisms of devastating earthquakes, volcanic eruptions and the associated hazard by imaging tectonic features. Likewise, it is an essential goal in sustaining the energy supply of human kind by exploring and monitoring georeservoirs (e.g. oil, gas, hydrocarbon, water).

Seismic tomography has been used towards this goal for many decades using e.g. teleseismic phases or surface waves generated by earthquakes for exploring the Earth's interior even deep down to the core. Controlled-source experiments utilizing e.g. explosives are frequently applied to image shallow crustal Earth in both continental and oceanic lithosphere.

Active-source seismic experiments such as wide angle or time-lapse seismic, using reflection/refraction methods are performed to investigate the regional crustal or basin structures. The depth resolution in seismic experiments is often controlled by the length of the source-receiver geometry and the strength of the source. Both have limits especially in urban environments. Moreover, these experiments require huge investments in case of time-lapse studies even involving repetitive usage of explosives or air guns that are environmentally unfriendly or questionable.

Due to the increase in high-quality digital data recorded by widely distributed broadband seismic stations and drastic improvement in 2D/3D computational tools, there is an evident progress in imaging the Earth at varying depths from local to

global scales with traditional tomography methods that use arrival times, amplitudes of seismic phases or even full waveforms. Among these, surface wave tomography has been successfully applied in retrieving the structure of the Earth's crust and upper mantle (e.g. Pasyanos et al., 2002; Trampert and Woodhouse 2007; Ritzwoller and Levshin 2012). Surface waves have large amplitudes over a wide range of periods. They propagate along extended paths with relatively low attenuation compared to body waves. The surface waves at different wavelengths penetrate down to different depths and propagate at the velocity of the medium they sample. This dispersive nature of surface waves allows one to invert for S-wave velocity structure of the medium.

However, earthquake based tomography studies require high local/regional seismicity rates and a dense source-receiver geometry to sufficiently sample the region of interest. In case of low seismic activity, the ray-coverage is usually limited and therefore the resolution is low. To overcome the problem of scarce earthquake-station distribution, using the ambient noise field that is ubiquitous all around the Earth has been introduced. Recordings of ambient noise field provide a continuous database to image both shallow and deep structures using surface and even body waves (Prieto et al., 2011). The cross-correlation of long-term ambient noise recordings for different station pairs can be used to estimate the Green's function of the surface wave propagation and thus to study the Earth structure at a well-resolved scale (Shapiro and Campillo, 2004).

This thesis comprises two case studies on the use of ambient seismic noise in terms of spatial and temporal sampling of the Earth' s crustal properties in the absence of earthquakes or active sources. In the first study, the uppermost crustal structure of a

local tectonic setting just prior to an expected major earthquake is investigated to better understand the structural asymmetry in the area of interest and to improve the resolution of hypocenter determination for local seismicity. Moreover, the feasibility of the approach is presented. Some fundamental questions addressed in this case study are as follows:

1. Can we identify and structurally characterize sedimentary basins by extracting the dispersion information of surface waves from ambient noise recordings?

2. Does obtaining an S-wave velocity model for a region defined only by a P-wave velocity model improve the precision in hypocenter determination?

The second case study is an example of temporal sampling of the Earth's crustal properties. The main focus is to monitor changes of the crustal velocity field associated with a major earthquake occurring in a very complex tectonic setting. The following fundamental questions are addressed in this case study:

1. Are there any coseismically introduced temporal changes of the crustal velocity field in response to a M+7 earthquake?

2. If so, can this velocity change be related to the spatial distribution and amount of coseismic slip?

The above-mentioned questions are addressed in this thesis by exploiting the dispersive nature of surface waves constituting the ambient noise field. The obtained results led to two peer-reviewed ISI-publications, one in *Bulletin of Seismological Society of America* and one in *Geophysical Research Letters*.

The thesis comprises the following chapters:

Chapter 2 gives an overview of the theoretical background as well as a brief introduction on the nature of ambient seismic noise.

Chapter 3 gives an overview of the tectonic setting of the two study regions in eastern and northwestern Turkey. The evolution and importance of the North Anatolian Fault Zone (referred to as NAFZ hereafter) in the Sea of Marmara region are shortly summarized. Moreover, the continent-continent collision within the Alpine-Himalayan orogenic belt, which led to the development of the NAFZ and the East Anatolian High Plateau, is briefly introduced.

Chapter 4 describes the first case study including a detailed description of the ambient noise cross correlation technique that is applied to identify the S-wave velocity structure of the Eastern Sea of Marmara region, Turkey. The main aim is to determine the seismic velocity field in the region where the main branch of the North Anatolian Fault Zone (NAFZ) is in the final phase of its seismic cycle and thus presumably just prior to an expected major earthquake offshore Istanbul. Low velocity zones related to the sedimentary fill of Çınarcık and Thrace Basins are observed in group velocity dispersion curves. A 1-D S-wave velocity model is obtained from an average dispersion curve for the target area and 1000 local earthquakes are relocated using this model. With the derived improvement in the hypocenter determination, it is presented that a reliable S-wave velocity model for the target area is an important input in further seismotectonic studies.

Chapter 5 comprises a study to investigate potential temporal variations in seismic velocity associated with the 2011 M7.1 Van, eastern Turkey, earthquake in order to

better understand the response of the Earth' s crust to a major event. A coseismic velocity decrease directly related to the Van mainshock is observed in the near vicinity of the earthquake hypocenter at three different frequency sub-bands. There is a clear correlation between the magnitude of the velocity decrease and the distance to the earthquake hypocenter and amount of coseismic slip on the rupture plane.

Chapter 6 summarizes the main findings of this thesis and gives a conclusive discussion as well as an outlook for recommended future investigations.

Chapter 2

Theoretical Background

2.1 Ambient seismic noise

On a typical seismogram, we observe direct waves as distinct phases, outcome of the deterministic, transient energy of the earthquakes and later a more complicated seismic coda, which is random and a result of multiple scattering of the propagating wavefield. Beside these, we observe seismic ambient noise due to Earth's surface continuous vibrations over a wide frequency range providing continuous sampling of the Earth's interior at different scales.

Ambient noise can be induced by natural or anthropogenic sources (Asten, 1978; Asten and Henstridge, 1984). The long period range of the noise spectrum is covered by the microseisms representing the response of typical natural sources (e.g. atmospheric disturbances or interaction of ocean waves with the coastlines). The microseism spectrum exhibits two strong peaks; primary (single frequency) microseism and secondary (double frequency) microseism. The primary microseism propagates at similar periods with the ocean waves (10–20 s) generated by the ocean-gravity waves near the coast (Hasselmann, 1963), while the secondary microseism propagates with half the period of ocean waves (5-10 s) originating from the nonlinear interaction between direct and reflected ocean waves (Longuet-Higgins, 1950). The short period range is predominantly characterized by microtremors resulting from cultural sources, such as traffic, industry and pipelines or from local meteorological events. Due to attenuation, cultural noise cannot propagate over large distances laterally and especially in vertical direction. Therefore, the signal to noise ratio is

usually high in boreholes and deep tunnels compared to surface recordings. The transition range between the frequency content of microseisms and microtremors is not sharp and might vary regionally (Bonnefoy-Claudet et al., 2006). Amplitude variations of microseisms are mostly controlled by oceanic activity or large-scale meteorological events, while the amplitude of microtremors may exhibit substantial man-made changes on daily or weekly basis.

The ambient noise wavefield is predominantly composed of Rayleigh and Love wave energy within a wide frequency range (Toksöz and Lacoss, 1968; Horike, 1985; Bonnefoy-Claudet et al., 2006). However, in practice, the frequency spectrum might also include body wave energy that might lead to artificial observations and therefore has to be taken into consideration during the analysis. The content of different wave types (body and surface waves, Rayleigh or Love fundamental or higher modes) strongly depends on site conditions and orientation of a particular seismometer as well as the source properties (Bonnefoy-Claudet et al., 2006).

By utilizing the correlation of ambient noise recordings, the dispersive nature of the surface waves can be extracted and used to obtain the shear wave velocity at varying depths and scales.

2.2 Passive imaging with ambient noise

Since the pioneering work of Aki (1957), azimuthal averaging of short inter-station distance correlations of noise to determine phase velocities of surface waves, different array processing and cross correlation techniques have been developed to obtain the dispersion relation in order to investigate S-wave velocity structures from recordings of ambient noise. The **SP**atial **A**uto**C**orrelation method (SPAC; Aki 1957) and the

frequency wavenumber (*f-k*) method (Capon et al., 1967; Capon, 1969; Lacoss et al., 1969; Kværna and Ringdahl, 1986) are the most common array-based approaches used for investigating the structure right below a deployed seismometer array (Aki, 1965; Henstridge, 1979). These approaches are mainly used in investigating shallow S-wave velocity structure, a crucial input in geotechnical and earthquake engineering studies (e.g. Hough et al., 1992; Malagnini et al., 1993; Friedrich et al., 1998; Liu et al., 2000; Bettig et al., 2001; Saccorotti et al., 2001; Kudo et al., 2002, Ohori et al., 2002; Scherbaum et al., 2003; Chavez-Garcia et al., 2005; Asten 2006; Köhler et al., 2007; Claprood and Asten, 2009; Claprood et al., 2011). Since there is no need to wait for an earthquake or use an active source, these methods are referred as Passive Imaging Techniques.

In seismology, Shapiro and Campillo (2004) used the long-term correlations of ambient noise recordings between two stations to estimate the surface wave Green's function, for the first time, in order to study the Earth structure. Historically speaking, in 1968, Claerbout proposed, the daylight imaging method (daylight data: a seismic data recorded on the Earth's surface generated by randomly distributed sources in the Earth), showing that the autocorrelation of a transmission response in a horizontally layered medium is the superposition of reflection responses. The source can be a transient or noise signal. This further inspired the author to generate 3D seismograms and to his conjecture that the cross-correlation of daylight traces recorded at two surface locations A and B, results in a reflection trace at B generated by a virtual source at A. Claerbout's conjecture was demonstrated later by Duvall et al., (1993) in helioseismology. The cross correlation of the Sun's random surface motion was used to obtain the time-distance curves on the solar surface. The conjecture was proven mathematically by Wapenaar (2003); Snieder (2004); Wapenaar (2004) in acoustic

media using elastodynamic respresentation theorem; by Weaver and Lobkis (2004) using the modal representation of the diffuse fields; by Wapenaar and Fokkema (2006) in both acoustic and elastodynamic media without any assumption on the diffusivity on the wavefield. Several more theoretical studies were carried out to further develop the ambient noise cross correlation technique (Larose et al., 2004; Shapiro and Campillo, 2004; Gouedard et al., 2008; Bensen et al., 2007).

Moreover, to demonstrate the feasibility of this approach, several laboratory experiments were performed (Lobkis and Weaver, 2001; Weaver and Lobkis, 2001; Derode et al., 2003; Larose et al., 2004). In laboratory acoustics, it has been shown how diffuse thermal noise recorded and cross-correlated at two transducers fastened to one face of an aluminum sample provided the complete Green's function between these two points (Weaver and Lobkis, 2001). They have explained their results with the use of equipartitioning of the modes. Moreover, Lobkis and Weaver (2001) showed that the multiple scattering in a heterogeneous medium could also produce random noise sources. Later, in a time-reversal experiment in the laboratory Derode et al., (2003) demonstrated that the reconstruction of the Green's function from the cross correlations of the ultrasonic wavefield is possible in an open scattering medium with absorbing boundary conditions and in a closed cavity with perfectly reflecting boundary conditions.

Further developing these approaches, Campillo and Paul (2003) stacked the cross correlations of seismic coda of 101 teleseismic earthquakes recorded in Mexico and showed that the diffuse waves emitted by these teleseismic sources are sufficient to retrieve Green's function between two stations. The work done by Campillo and Paul (2003) opened the way for many follow-up studies in this field. For example: in ocean

acoustics where both direct and reflected wavefronts are retrieved from ambient noise cross correlation (Roux and Kuppermann, 2005) or in investigating the lunar subsurface structure (Larose et al., 2005) or in geotechnical engineering (Snieder and Safak, 2006). The same approach is widely used to derive structural 3-D models of basin and subduction zones or to conduct ground motion simulations at active plate boundaries. Ambient noise tomography has been applied to investigate the crustal/uppermost mantle structure (Sabra et al., 2005; Shapiro et al., 2005, Yao et al., 2006; Lin et al., 2008; Brenguier et al., 2007; Moschetti et al., 2007; Yang et al., 2007; Bensen et al., 2008; Yang and Ritzwoller, 2008; Saygin and Kennett, 2010; Zheng et al., 2010; Warren et al., 2013). This technique is also applied in the marine environment using ocean bottom stations to model the shallow shear wave velocity structure in the south central Pacific (Harmon et al., 2007), to retrieve the 3-D velocity model for local landslides in the area of Avignonet (France) (Renalier et al., 2010), to locate a scatterer in the volcanic area of southern Peru (Ma et al., 2013), to measure the basement seismic resonance frequency in shallow structures (Savage et al., 2013), to retrieve body waves (Roux et al., 2005) and to image the mantle transition zone (top: 410 km and bottom: 660 km) from the correlations of body waves (Poli et al., 2012).

2.3 Passive monitoring with ambient noise

Another long time goal of seismologists is to measure and monitor changes in stress and strain fields associated with large earthquakes in order to further develop earthquake forecasting or seismic hazard and fault-zone characterization. In the seismogenic crust, a better knowledge on the temporal changes is also crucial to better understand the rock rheology and therefore to better estimate the site response.

Several laboratory studies have shown that the rock properties (e.g. seismic velocity, attenuation, anisotropy) vary due to changes in the stress field (Scholz, 1968; Nur and Simmons, 1969; Chesnokov and Zatsepin, 1991; Birch, 1966; Crampin and Zatsepin, 1997).

During a major earthquake, strain energy accumulated over hundreds of years is released in a few seconds. This short-term drastic change in the stress field is abruptly reflected as deformation in the elastic parameters of the medium. Crustal properties deform also near active volcanoes as a result of eruptions and volcano evolution. Using traditional seismological approaches these temporally varying seismic properties can be measured. Surface deformation is observed successfully using GPS and strainmeter data. However, to measure the depth distribution of changes in stress field is difficult to achieve. Early attempts of monitoring these changes include using the travel time of P and S and/or V_p/V_s ratios (e.g. Whitcomb et al., 1973), seismic anisotropy (e.g. Crampin et al., 1990) and the analysis of amplitude of the coda waves (e.g. Aki, 1985; Jin and Aki, 1986). However, due to the uncertainties in the earthquake locations and origin times, these observations are not found reliable (Kanamori and Fuis, 1976; Beroza et al., 1995; Peng and Ben-Zion, 2005). Following the improvements in the earthquake relocation techniques based on waveform cross correlation (e.g. Schaff et al., 1998) and the double difference algorithm (e.g. Waldhauser and Ellsworth, 2000), relative earthquake locations are significantly improved as well, opening the way for e.g. using the coda part of repeating earthquakes (natural sources) to monitor stress induced crustal changes (Poupinet et al., 1984; Schaff et al., 1998; Baisch and Bokelmann, 2000; Schaff and Beroza, 2004; Peng and Ben-Zion, 2005; Sawazaki et al., 2009; Yu et al., 2013). Repeating earthquakes regularly occur on the same patch of the fault plane, producing almost

similar waveforms recorded at the same receiver. Their existence mainly depends on the amount of loading creep rate and rock properties (Cheng, 2008). They usually have the same magnitude, same source mechanism and approximately the same repeating interval. Besides monitoring coseismic and aseismic temporal changes in the seismic velocity, they are widely used to study the rupture size. However, the occurrence of repeating earthquakes (especially a pre-event before the mainshock) in the region of interest and their temporal coverage are limited. Instead, by using controlled sources artificially repeating events can be produced. Repeating shots are used to monitor changes with more accurate source, location and time information (Li et al., 1998; Nishimura et al., 2005; Vidale and Li, 2003). Nevertheless, these studies have limited depth penetration, especially for studies of physics of the earthquakes, and limited temporal sampling. Moreover, active source experiments are environmentally questionable.

Using either an active or a natural source, the two early approaches to the problem of monitoring the velocity change are; measuring the variations in the travel times of the first arrivals and comparing P-, S-wave coda. In a strongly scattering medium, the waves repeatedly sample the same region in space and such a medium acts as a natural interferometer (Snieder, 2006). These multiply scattered waves are more sensitive to small changes in a medium then the ballistic waves and appear as seismic coda in a seismogram. A small change in velocity results in a time shift increasing proportionally with the lapse time. Since seismic coda waves are multiply scattered waves with longer propagation paths the later part of the coda will accumulate more delay (Snieder, 2002). The application of seismic interferometry to coda waves is named as coda wave interferometry (CWI). The CWI is tested under laboratory conditions by Snieder et al., (2002). The authors measured the velocity change on a

granite sample with temperature and detected a change of ~0.1%. Gret et al., (2006) applied coda wave interferometry on rock samples to investigate the wave velocity variation due to variations in stress, temperature and water saturation under laboratory conditions. Pandolfi et al., (2006) applied CWI to the 1999 M3.6 Mt. Vesuvius event and measured velocity changes smaller than 0.4%.

Monitoring the stress-induced velocity change requires identical excitation of an unperturbed and a perturbed signal (Snieder, 2006). For this purpose, repeating natural or active sources are used which both have disadvantages as mentioned before. Seismic ambient noise field that is ubiquitous all around the Earth provides a completely continuous database for monitoring studies and an undisturbed source area. There are two main approaches exploiting the seismic coda of the ambient noise field to monitor temporal changes. One is the doublet technique proposed by Poupinet et al., (1984) in which the shift between two recordings is measured in a limited time window centered at a time t. This procedure will be repeated at different times and the average slope of the delay versus time plot results in the variation in velocity (dV/V). The other one, stretching interpolation technique, interpolates the coda times at shifted times related to various velocity changes in a certain time window. This is relevant to stretching or compressing the time axis. The actual velocity change can be calculated when the best fit between the stretched/compressed and the original coda is obtained. Sens-Schönfelder and Wegler (2006) applied coda wave interferometry (CWI) technique, using ambient noise field to monitor seasonal variations of seismic velocity at Merapi volcano and named the technique as passive image interferometry (PII). Wegler and Sens-Schönfelder (2007) detected a 0.6% decrease in coseismic velocity by analyzing the autocorrelation function of ambient noise field recorded at a station located in the rupture zone of the 2004 Mid-Niigata earthquake. Extending this

work to more seismic stations in the region and both cross- and auto correlating the ambient noise field Wegler et al., (2009) identified a velocity decrease of 0.5%. Many more authors applied this technique to monitor temporal changes in the crust associated with major earthquakes e.g., Brenguier et al., (2008) for M6.5 2003 San Simeon and M6.0 2004 Parkfield earthquakes; Chen et al., (2010) for 2008 M7.9 Wenchuan earthquake; Zaccarelli et al., (2011) for 2009 M6.1 L'Aquila earthquake; Hobiger et al., (2012) 2008 M6.9 Iwate-Miyagi earthquake; Minato et al., (2012) for 2011 Tohoku-Oki earthquake, Liu et al., (2014) for 2008 M7.9 Wenchuan earthquake by using 3-component ambient noise recordings. All of these authors reported a coseismic velocity decrease associated with the corresponding earthquake. Velocity changes related to volcanic eruptions are observed by Brenguier et al., (2008) at Piton de la Fournaise volcano on Reunion Island. Rivet et al., (2011) investigated the 2006 M7.5 slow slip event in Guerrero, Mexico and associated the observed mid-crustal velocity changes with the strain rate rather than the strain itself.

2.4 Green's function estimation

The main aim of ambient noise cross correlation technique, which appears in a wide range of different disciplines, is to reconstruct the Green's function of a medium. Mathematically, the Green's function provides an important tool for solving differential equations (in this case wave equation) that are particular to each specific problem. Simply, we can define it as the response of a medium to an impulsive source.

The cross-correlation of a fully diffuse wavefield (isotropic random waves propagating with equal power in all possible directions) computed between a pair of receivers, would result in a waveform that differs only by a smooth frequency

dependent amplitude factor from the Green's function of the medium between the receivers (Weaver and Lobkis, 2001; Lobkis and Weaver, 2001; Weaver and Lobkis, 2004; Wapenaar, 2004; Shapiro et al., 2005; Snieder, 2004; Sanchez-Sesma et al., 2006) (Figure 2.1). This is a complete Green's function of the medium that is symmetric in time, including all reflections, propagation modes and scattering. All these authors come to this conclusion by addressing the problem with equivalent assumptions either about the noise wavefield or sources.

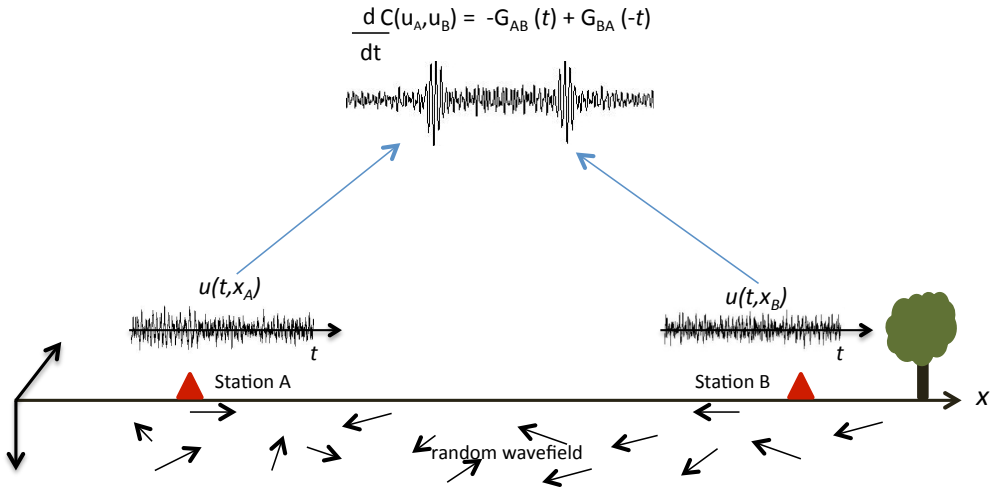

Figure 2.1 Illustration of ambient noise cross correlation (after Weaver, 2005) and the definition of variables. The Green's function of a medium between two points *A* and *B*, represents the wavefield recorded at *A* for an event that occurred at *B*.

One of these theoretical approaches assumes that the wavefield is composed of white noise distributed everywhere in the medium without any assumption about the medium. Following Gouedard et al., (2008), the time domain cross correlation C between the displacements at points A ($u(t,\vec{x}_A)$) and B ($u(t,\vec{x}_B)$) can be written as

$$C(\tau,\vec{x}_A,\vec{x}_B) = \lim_{T\to+\infty}\frac{1}{T}\int_0^T u(t,\vec{x}_A)\overline{u(t+\tau,\vec{x}_B)}dt \qquad (1)$$

where the bar denotes the conjugate. The displacement can be expressed using the Green's function G_a (includes "a", a constant for the attenuation factor ($a > 0$), to ensure the convergence of the integral (Roux et al., 2005)) as

$$u(t,\vec{x}) = \int_0^\infty dt' \int_R G_a(t',\vec{x},\vec{x}_s) f(t-t',\vec{x}_s) d\vec{x}_s \qquad (2)$$

where f is the source time function assumed to be a white noise distributed everywhere in the medium R, acting at any time t.

$$C(\tau,\vec{x}_A,\vec{x}_B) = \lim_{T\to\infty} \frac{1}{T} \int_0^T dt \int_0^\infty ds \int_R d\vec{x}_s\, G_a(s,\vec{x}_A,\vec{x}_s) f(t-s,\vec{x}_s) \qquad (3)$$

$$\times \int_0^\infty ds' \int_R d\vec{x}_s\, \overline{G_a(s',\vec{x}_B,\vec{x}_{s\prime}) f(t+\tau-s',\vec{x}_{s\prime})}$$

A white noise contains all the frequencies with a random phase in the frequency domain. In the time domain, this is a random wavefield such that the position and the activation time of each source are uncorrelated. In this case, the limit T can be replaced by the ensemble average $\mathbb{E}$

$$\lim_{T\to+\infty} \int_0^T f(t-s,\vec{x}_s)\, f(t+\tau-s',\vec{x}_{s\prime}) dt = \mathbb{E}[f(t-s,\vec{x}_s) f(t+\tau-s',\vec{x}_{s\prime})] \qquad (4)$$

$$= \sigma^2 \delta(\tau+s-s') \delta(\vec{x}_s - \vec{x}_{s\prime})$$

where σ is the variance of the white noise. By using this property, equation (3) can be simplified to

$$C(\tau,\vec{x}_A,\vec{x}_B) = \sigma^2 \int_0^\infty ds \int_R d\vec{x}_s\, G_a(s,\vec{x}_A,\vec{x}_s) \overline{G_a(s+\tau,\vec{x}_B,\vec{x}_s)} \qquad (5)$$

In case of an attenuating medium, by using a negative definite elliptic differential operator, the time derivative of equation (5) results in the positive and negative lags of the Green's function

$$\frac{d}{dt}C(\tau,\vec{x}_A,\vec{x}_B) = \frac{-\sigma^2}{4a}(G_a(\tau,\vec{x}_A,\vec{x}_B) - G_a(-\tau,\vec{x}_A,\vec{x}_B)) \tag{6}$$

In general, this result means that for any medium the time derivative of the cross correlation computed between the wavefields recorded at stations A and B yields the Green's function of the medium with the assumption of the noise sources are located randomly anywhere in the medium and active at any time (Figure 2.1). There is another approach based on equipartitioning without making any assumptions about the location or activation time of the noise sources (Weaver and Lobkis, 2001). The only assumption is that there is equipartitioning at the boundaries of the region of interest, that eigenmodes of the system (normal modes of the Earth) are uncorrelated and excited at the same level of energy. As an alternative approach, equipartitioning can be satisfied by employing the embedded scatterers as secondary sources thus yielding multiple scattering of the wavefield (Snieder, 2004). In practice, multiple scattering of seismic waves compensates for the lack of noise sources, therefore the randomness can be produced both by the distribution of sources or by scattering of seismic waves by topography and internal sources (Stehly et al., 2008).

2.5 Data Processing

Information on the Earth structure can be extracted from the correlations of ambient noise recordings using the relation between the cross correlation and the Green's

function as expressed in Equation 6. This computation is based on some assumptions about the noise wavefield such as diffusivity and equipartitioning. However, in real Earth these assumptions are not satisfied. To overcome this, averaging over long period correlations and some additional pre-processing to raw data are applied. The choice of pre-processing steps depends on the data and aim of the study and therefore may vary. Once a uniform database of daily continuous ambient noise recordings for each station is prepared, general data processing steps to be applied are summarized in Bensen et al., (2007). Data processing is applied in four steps; (1) preparing single station data before cross correlation, (2) cross correlation of possible station pairs and stacking, (3) dispersion measurement, (4) error analysis and data selection. The first step is the preparation and pre-processing of single station waveform data, e.g. removing the mean, trend, instrument response and bandpass filtering. In addition to these, undesired effects of earthquake signals, nonstationary noise sources nearby the stations and instrumental irregularities need to be removed. For this purpose, temporal normalization is applied to the data. Bensen et al., (2007) have proposed five different methods for removal of such contaminants. The first one is one-bit normalization method in which only the sign of the raw signal is kept by replacing all positive amplitudes with "+1" and all negative amplitudes "-1" (Campillo and Paul, 2003; Shapiro and Campillo, 2004; Yao et al., 2006). The second one is applying a clipping threshold equal to the RMS amplitude of the signal for a daily recording (Sabra et al., 2005). The third method is an automated event detection and removal if the amplitude of the waveform is above a critical threshold. The fourth one is computing the running average of the absolute value of the waveform in a normalization time window of a fixed length and weighting the waveform at the center of the window by the inverse of this average. This is called water-level normalization in which any amplitude above

a specified multiple of the daily RMS amplitude is down weighted. This method need to be run iteratively until the whole waveform is below the water-level therefore is the most time consuming one. In the frequency domain, ambient noise is not flat, as explained in a previous section there are peaks (primary and secondary) in the microseism band, also some rises at long periods above 50s due to Earth's hum. By applying a spectral normalization, which inversely weights the complex spectrum by a smoothened version of the amplitude spectrum, a whitened spectrum is obtained and the frequency band of the ambient noise signal is broadened. The pre-processing steps applied in this study are shown in Figure 2.2.

The next step after preparing the daily ambient noise recordings is cross correlation and stacking. As mentioned before, to reconstruct the exact Green's function, a homogeneous and random distribution of noise sources is necessary. However, in real Earth these conditions are impossible to satisfy. The distribution of the noise sources can be homogenized by using long time series in correlations. Usually, the correlations are computed between all station pairs, corresponding to $n(n-1)/2$ correlations where n is the number of stations. The resulting cross correlations are two sided time functions with positive (causal) and negative (acausal) correlation lags. If the noise sources are homogeneously distributed in azimuth then the causal and acausal correlation lags will be identical. Asymmetry in the amplitude and the spectral content of the correlations is observed due to the inhomogeneous distribution of the noise sources and the differences in the noise processes. Stacking over long time series significantly improves the signal to noise ratios, however even after averaging over one year of seismic noise recordings, the desired symmetry may not be obtained. Moreover, if the station pairs are poorly oriented with respect to the dominant direction of the noise source, the extraction of fundamental mode of surface waves

can be difficult. Furthermore, if the station quality is poor so the estimated Green's functions. As a result, in tomography studies, less than one third of the correlation paths are used (Stehly et al., 2008).

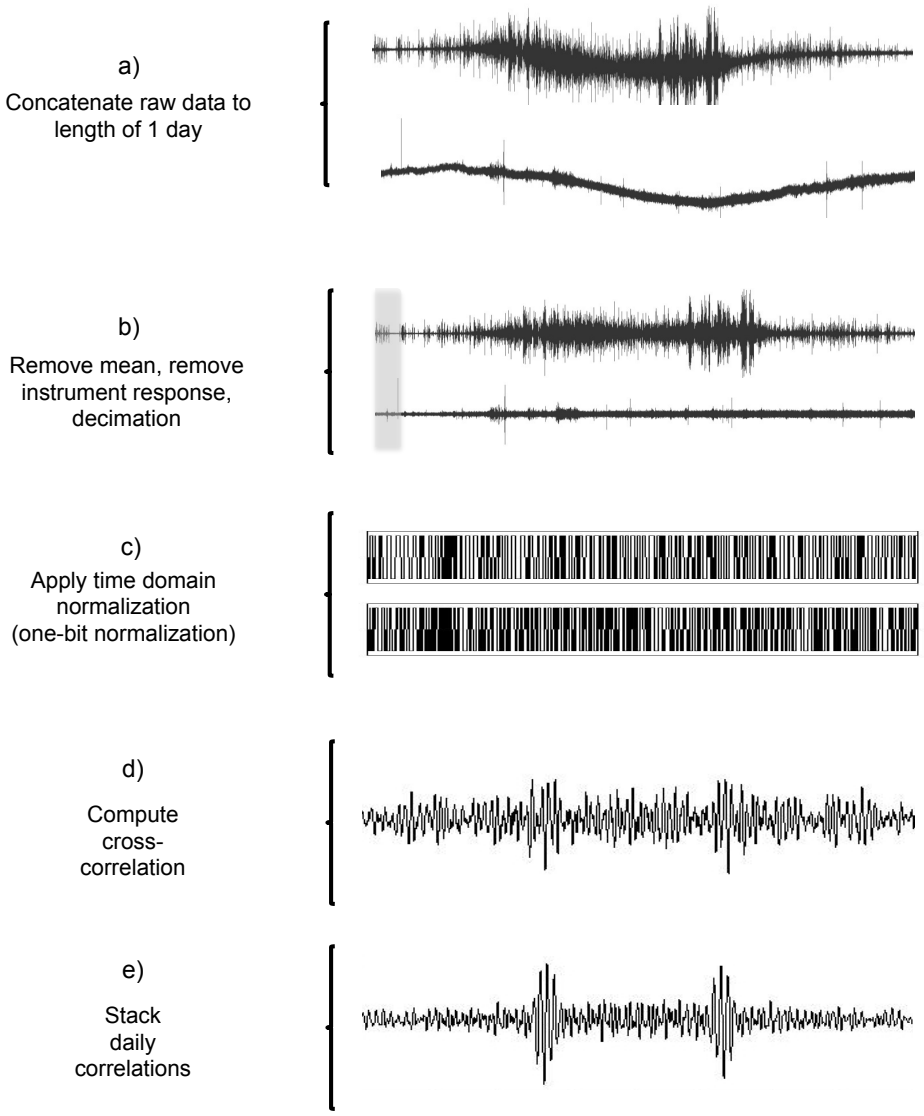

Figure 2.2. The data processing steps applied in this study are summarized schematically. a) Raw data example from a pair of stations, b) after de-meaning, -trending and instrument response removal, c) one-bit normalization applied to the data segment indicated with the shaded area in (b), d) cross correlation of the same data segment and in e) emergence of empirical Green's function after stacking are demonstrated.

The third stage is obtaining dispersion; the group/phase velocity as a function of frequency or period. This can be done by employing a system of narrow-band Gaussian filters, with varying central frequency to the cross correlations calculated in the previous step. The paths with interstation distances greater than three wavelengths should be taken into account for reliable dispersion measurements (Bensen et al., 2007). Once the arrival time of the cross correlation envelope at a certain frequency is determined, the group velocity can easily be computed for a known interstation distance.

The final step, quality control, can be performed by computing the signal to noise ratio, which can be increased by correlating as long time sequences as possible. Another indicator of a reliable measurement is determined by the repeatability in time. Ambient noise sources vary seasonally and provide different conditions for measurements. Within one or two-year long noise recordings, measurement uncertainty can be equated to seasonal repeatability (Bensen et al., 2007). Once the good quality group/phase velocity dispersion measurements are chosen, traditional surface wave tomography procedures can be applied.

Chapter 3

Tectonic setting

Within the context of this thesis, the ambient noise cross correlation approach is applied to ambient seismic noise recordings at two prominent locations along the North Anatolian Fault Zone in Turkey; the Istanbul/eastern Sea of Marmara region in northwestern Turkey, to determine the crustal structure and the Van region in eastern Turkey to monitor potential coseismic velocity changes associated with the M7.1 earthquake that occurred in 2011. In the following, the two regions of interest are introduced with respect to their seismotectonic setting.

3.1. Eastern Sea of Marmara Region, NW Turkey

The Sea of Marmara, covering an area of 11.350km^2, is located in northwestern Turkey, between the Black Sea in the north and the Aegean Sea in the southwest. It is an intra-continental marine basin with a broad shallow southern shelf and a deep northern part. The northern part includes three sub-basins; Çınarcık (~1250m deep), Central (~1220m deep) and Tekirdağ (~1112m deep) basins from east to west, respectively. These basins are separated by two NE-trending transpressional ridges; the Western and Central highs.

The eastern Sea of Marmara has a key position in this study since it accommodates the continuation of the North Anatolian Fault Zone (NAFZ), the Princes' Islands segment as the main fault branch located offshore Istanbul. The Princes' Islands segment is currently in the final phase of the seismic cycle prior to an expected major earthquake.

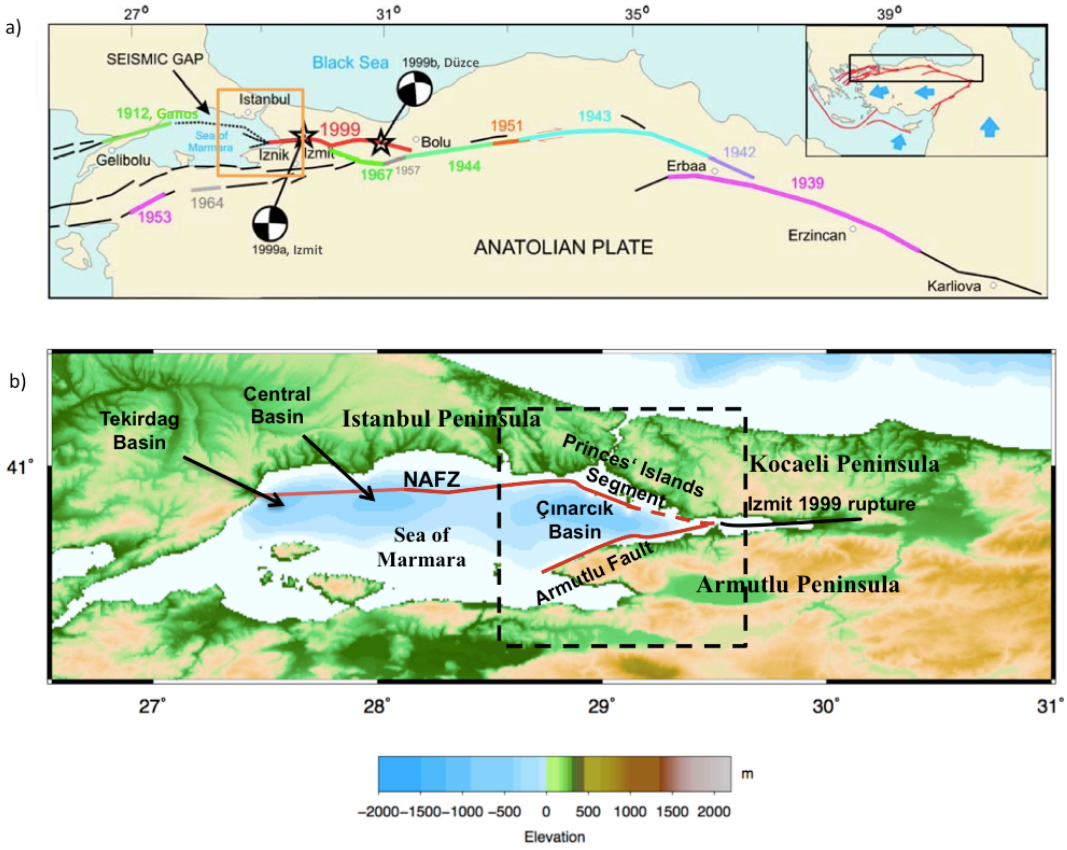

Figure 3.1 a) Tectonic map of NAFZ and Marmara region (after Bulut et al., 2009). Rupture zones associated with major earthquakes that occurred due to the westward movement of Anatolian plate along NAFZ are represented in different colors. b) The Sea of Marmara region in northwestern Turkey, with major tectonic elements and the main branches of NAFZ (NAFZ: red lines). The bold black line shows the western part of the 1999 Izmit earthquake rupture. In both figures the target area is framed with a black-dashed box. (Topography, SRTM30 grid; bathymetry, Armijo et al., 2002.)

The NAFZ represents one of the most active plate-bounding strike-slip faults. It has developed in the tectonic frame of the northward moving Arabian plate and the Hellenic subduction zone where the African lithosphere is subducting below the Aegean, following the closure of Neotethys Ocean. It is ~1600 km long extending between eastern Anatolia and the North Aegean (Figure 3.1a), and predominantly forms a right-lateral strike-slip plate boundary that slips at an average rate of 20-30 mm/yr (e.g. Barka, 1992; McClusky et al., 2000). During the last century, the NAFZ has ruptured over 900 km of its length (Ambraseys, 1970; Barka, 1999).

The NAFZ was initiated in eastern Anatolia during Late Miocene and propagated westwards to Marmara Sea region during Pliocene (Şengör, 1979; Barka 1992; Okay 1999, Le Pichon et al., 2001). The earthquake in 1939 near Erzincan, eastern Anatolia, marks the beginning of a series of large earthquakes (1942 M6.9 Niksar, 1943 M7.7 Tosya, 1944 M7.5 Gerede, 1951 M6.9 Çankırı, 1957 M6.8 Abant, 1967 M7.0 Mudurnu) propagating westward (Figure 3.1a) towards the Istanbul-Marmara region in NW Turkey. This migration has so far ended with two most recent devastating earthquakes in 1999, the August 17 Izmit (M7.4) and the November 12 Düzce (M7.2), together rupturing an almost 200 km long portion of the NAFZ by activating several 30-40km long segments. The recent earthquake series along the NAFZ left over a >100 km long seismic gap below the Sea of Marmara, between the 1912 M7.4 Ganos (western Marmara) and 1999 M7.4 Izmit ruptures (e.g. Toksöz et al., 1979; Stein et al., 1997; Reilinger et al., 2000). This segment did not rupture since 1766 and is believed to be capable of generating several M7 earthquakes (Hubert-Ferrari et al., 2000) or possibly a number of en-echelon normal faulting events (Armijo et al., 2002) within the next decades. According to Le Pichon et al., (1999), it can even rupture as a single strike-slip event by activating the so-called "Main Marmara Fault", crossing the entire Sea of Marmara. The 30-year probability estimation of an M+7 event in the Sea of Marmara is 35-70% (e.g. Wright et al., 2001; Parsons et al., 2000; Parsons, 2004).

The target area we aim to image is the eastern Sea of Marmara including the Princes' Islands segment of NAFZ, bounding the Çınarcık basin offshore of the large population center of Istanbul (Figure 3.1b). The western end of the 1999 Izmit rupture is located in the eastern Sea of Marmara below the Çınarcık Basin (e.g. Wright et al., 2001). It may have extended to just south of the Princes' Islands (Bouchon et al.,

2002; Özalaybey et al., 2002). The Çınarcık basin is a wedge-shaped half-graben representing a pull-apart basin oriented N110^{o} E in the eastern part of the Sea of Marmara. It covers an approximately 50x20 km wide area at a maximum seafloor depth of ~1250 m. The sediment fill reaches up to ~3.5 km (Karabulut et al., 2003; Carton et al., 2007).

3.2 Van Region, E Turkey

In the second part of this thesis, ambient noise cross correlations before and after the 2011 Van earthquake are analyzed. The city of Van was struck by a M7.1 earthquake on 23 October 2011. The epicenter lies in eastern Turkey (Figure 3.2a) and is not directly linked with the NAFZ. The broader Van region is defined as a seismically active zone where devastating earthquakes can occur. The 2011 mainshock caused a significant damage in the city of Van and surrounding villages, with 604 fatalities and 2608 injuries according the Prime Ministry Disaster and Emergency Management Presidency (AFAD, www.afad.gov.tr). The M5.7, 9 November 2011 aftershock, which can be associated with the main event, also caused additional 644 fatalities in the area (Erdik et al., 2012).

The region surrounding the city of Van, East Anatolian High Plateau, has a very complex tectonic setting. It is one of the youngest active continent-continent collision zones in the Alpine-Himalayan orogenic belt. The region accommodates an elevated morphology of ~1.5 – 2 km above sea level (Keskin et al., 2003) due to the continental collision between stable Eurasia and the northward-migrating Arabian plate (Şengör and Yılmaz, 1981). The collision initiated after the closure of the southern branch of the Neotethys Ocean at around 15 Ma. The volcanism due to the collision started after the closure in the north of the present day Lake Van. Both, the

continental collision and the magmatism are still ongoing processes, because the Arabian plate still converges to Anatolia (Keskin et al., 2003).

Operating together with the volcanism, tectonic activity led to the development of three main plate boundaries in eastern Turkey are the right-lateral NAFZ, the left lateral East Anatolian Fault Zone (EAFZ) and the Bitlis-Zagros Suture Zone (BZST) (Figure 3.2a-b). Beside these, the region accommodates east-west oriented thrust fault zones, northwest-southeast oriented right lateral and oriented northeast-southwest left lateral fault zones (Şaroğlu et al., 1992). The largest earthquakes recorded in the region are the 1903 M7.0 Ercis and 1976 M7.2 Çaldıran earthquakes. There are also reports of 1715 Ercis and 1646-1648 SE of Lake Van destructions from the pre-instrumental period (Ambraseys, 1989). The tectonic evolution and thus the complexity of the target area provide an interesting laboratory to study the potential variations in seismic velocity associated with a major earthquake.

The crust and lithosphere beneath the East Anatolian High Plateau is anomalously thin (Zor et al., 2003). The uppermost mantle can be represented by strong Sn attenuation, slow shear and Pn velocities (Gök et al., 2003; Gök et al., 2007; Al-lazki et al., 2003). Moreover, there are no subcrustal earthquakes and the crustal seismicity is predominantly strike-slip indicating that the convergence is due to tectonic escape (Türkelli et al., 2003; Örgülü et al., 2003). All these geophysical observations summarize the tectonic evolution of East Anatolian Plateau, suggesting slab detachment around 11 Ma and subsequent emplacement of hot asthenosphere at subcrustal depths supporting the high topography (Şengör et al., 2003).

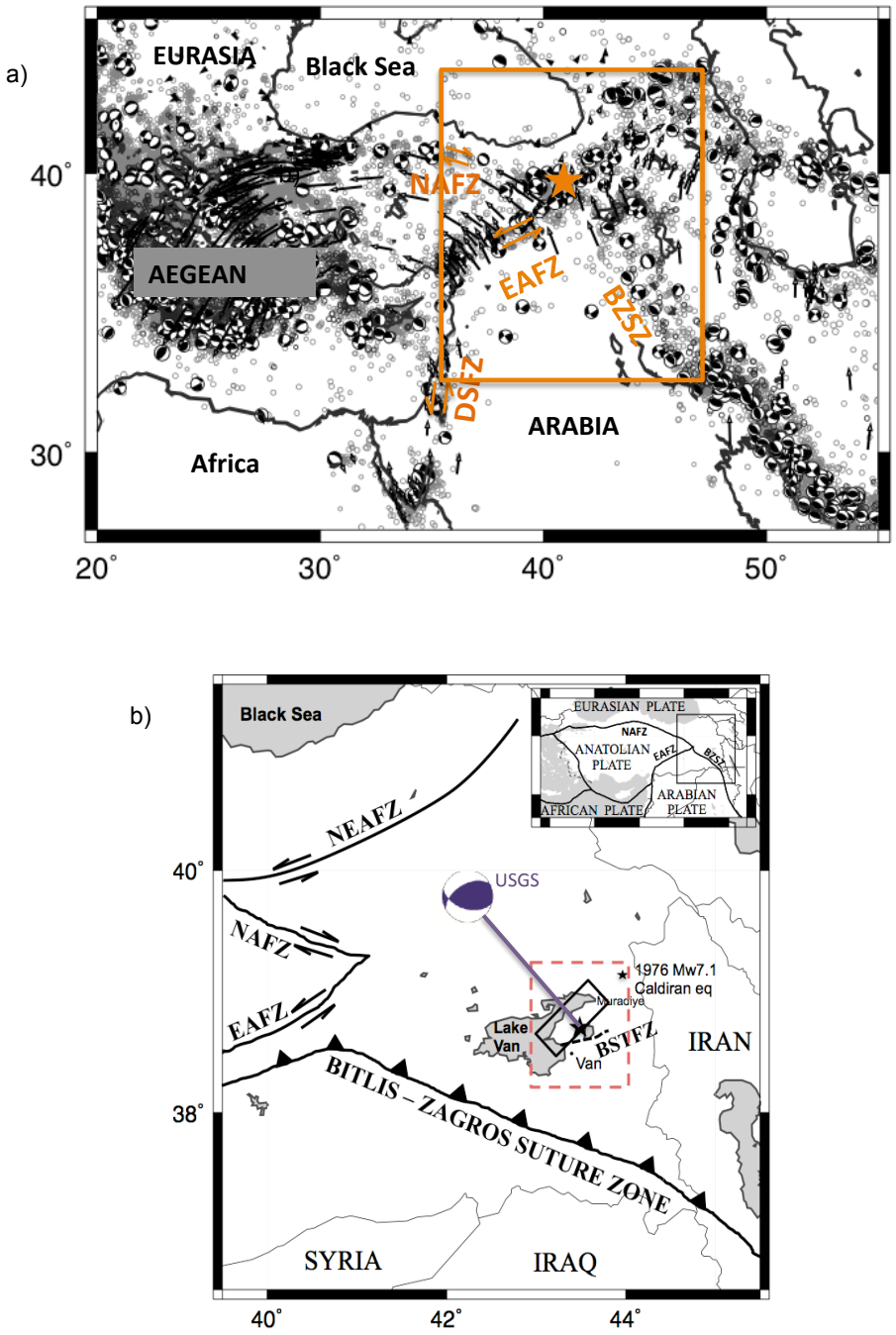

Figure 3.2 a) Seismotectonic setting of greater Anatolian-Aegean region. The major tectonic features are presented; right lateral North Anatolian Fault Zone (NAFZ), left lateral East Anatolian Fault Zone (EAFZ) and the Bitlis-Zagros Suture Zone (BZST). The orange box frames the East Anatolian High Plateau. b) Tectonic setting of the enlarged target area framed in (a). (NEAFZ: Northeast Anatolian Fault Zone, BSTFZ: Bardakçı-Saray Transform Fault Zone)

The 2011 Van earthquake occurred off the main plate boundary on the Bardakçı-Saray Thrust Fault Zone (Figure 3.2b) that was not identified on the active fault map of Turkey (Şaroğlu et al., 1992). The surface rupture is limited to a length of 8 km, indicating that most of the mainshock slip occurred below the surface. Therefore, the fault accommodating the 2011 Van earthquake has been interpreted to be a blind thrust fault to a large extent (Doğan and Karakas, 2013). The earthquake activated a reverse fault with a hypocentral depth of 16 km (http://www.usgs.gov) and a coseismic slip maximum of 4 m (Hayes, 2011). The rupture plane is striking NE dipping towards the NW in a NW-SE compressional stress field with a small left-lateral component (Doğan and Karakas, 2013).

The aftershocks are distributed mostly outside the nucleation zone extending beneath Lake Van in the west and towards the town of Muradiye in the east, near the epicenter of the 1976 Çaldıran earthquake (M 7.1). The region falling between the eastern tip of the 2011 Van aftershock activity and the 1976 Çaldıran rupture zone did not host a major earthquake since 1976 therefore probably represents a highly stressed fault segment (Akıncı et al., 2012).

Chapter 4

Ambient noise analysis in the eastern Sea of Marmara region in NW Turkey: Lateral variations of the crustal velocity field [1]

[1] Published in *Bulletin of Seismological Society of America*, as Acarel, D., Bulut, F. and Bohnhoff, M. (2014). Ambient noise analysis in the eastern Sea of Marmara region in northwest Turkey: Lateral variations of the crustal velocity field. doi: 10.1785/0120130160 http://dx.doi.org/10.1785/0120130160

Chapter 5

Coseismic velocity change associated with the 2011 Van Earthquake (M7.1): Crustal response to a major event[1]

[1] Published in *Geophysical Research Letters* as Acarel, D., Bulut, F., Bohnhoff, M., and Kartal, R. (2014). Coseismic velocity change associated with the 2011 Van earthquake (M7.1): Crustal response to a major event. DOI: 10.1002/2014GL060624

Summary

Monitoring co-seismic velocity changes is a major challenge, since the Earth crust has to be uniformly sampled at pre- co- and post-seismic stages using repetitive active or natural sources. Here, we investigate the crustal response to the 2011 Van earthquake using ambient noise, which provides the best-possible temporal resolution. Combined recordings from the nearest five broadband stations are analyzed for a time period of six months framing the mainshock. We observe a co-seismic velocity decrease of up to 0.76 % in the vicinity of the mainshock in the frequency range of 0.05 – 0.3 Hz. The velocity drop is largest at close proximity to the earthquake hypocenter and decreases systematically with distance. We find a correlation between co-seismic velocity decrease and the amount of co-seismic slip on the rupture plane. The observed velocity drop shows the drastic response of brittle crust in response to a major earthquake.

5.1 Introduction

Large earthquakes represent significant elastic responses of the brittle part of the Earth's crust as the strain energy accumulated typically over hundreds of years is released in a few seconds. This drastic short-term acceleration in deformation rate during a large earthquake diverts the near-fault damage, state of stress and pore pressure (e.g. Toksöz et al., 1976; Christensen and Wang, 1985; Vidale and Li, 2003). The compound of such changes is therefore abruptly reflected in the changes of elastic parameters of the surrounding medium such as e.g. seismic velocity (Rubinstein and Beroza, 2004).

Temporal changes of the seismic velocity have been studied for several decades using repeating earthquakes (e.g. Poupinet et al., 1984; Baisch and Bokelmann, 2001)) and explosions and aftershocks (e.g. Li et al., 1998; Nishimura et al., 2000). The principal study by Poupinet et al. (1984) verified a 0.2 % velocity drop following the M 5.9 Coyote Lake Earthquake in 1979 using comparison of coda waves from two repeating earthquakes. Theoretically, the seismic velocity might change even in case of small variations in the spatial distribution of scatterers (Snieder et al., 2002; Snieder, 2006). Such a perturbation modifies the observed seismic signals radiated by repeating earthquakes sampling the same source-receiver path at different time spots. However, the occurrence of repeating earthquakes is limited to a few specific regions resulting in a poor spatial coverage on a global scale and thus does not provide a generalized scheme for investigating potential temporal changes due to major earthquakes.

Time-lapse active seismic experiments have been proposed as an alternative approach to investigate temporal change of the seismic velocity field. Nishimura et al. (2000)

observed a 0.3-1.0 % decrease in velocity using two separate controlled-source experiments before and after the 1998 M6.1 Mount Iwate earthquake, respectively. Using repeated seismic profiles to monitor temporal velocity changes in the crust provides a reasonably good spatial resolution due to a controlled source-receiver geometry. However, such experiments involve huge costs and therefore do not represent a feasible tool for systematical analysis of earthquake-related changes of seismic velocity.

Since ambient noise is continuous in time and space, it provides an alternative tool to monitor potential temporal changes of the crustal seismic velocity. The emergence of Green's function from the correlation of diffuse wavefields between two sensors has been firstly demonstrated by ultrasonic and thermal noise laboratory experiments (Weaver and Lobkis, 200; Lobkis and Weaver, 2001). These methods have then been extended to field scale by Shapiro and Campillo, (2004) and Shapiro et al., (2005) by correlating the ambient noise field between two seismometers. Moreover, Campillo and Paul (2003) estimated Green' s function from the correlations of seismic coda waves. In another attempt, the emergence of the scattered waves from the correlations of seismic ambient noise was demonstrated by Sens-Schönfelder and Wegler, (2006). The basic idea behind these studies is to treat reconstructed Green's functions from cross-correlations of continuous ambient seismic noise recordings as a substitute for seismograms generated by e.g. repetitive earthquakes or active sources (Brenguier et al., 2008; Chen et al., 2010; Zaccarelli et al., 2011; Liu et al., 2014).

In this study, we investigate co-seismic velocity perturbations related to the M7.1 2011 Van earthquake, eastern Turkey, using ambient noise recorded July 2011 –

January 2012. We analyze velocity perturbations as a function of distance to the earthquake hypocenter and mainshock maximum slip along the ray-path, respectively, in order to further elaborate on the spatial distribution of elastic response of the Earth's crust to a M>7 earthquake. To capture potential velocity changes, we constructed cross-correlation functions from six month long continuous recordings of five local broadband framing the time of the mainshock.

5.2 The 2011 Van Earthquake

Eastern Turkey has been struck by a M7.1 earthquake, on 23 October 2011 occurring near the city of Van, east of the Karlıova triple junction (Figure 1). The earthquake activated a reverse fault with the hypocenter being located at 16 km depth (http://www.usgs.gov) and with a co-seismic slip maximum of 4 m (Hayes, 2011). The rupture plane is striking NE dipping towards the NW in a NW-SE compressional stress field with a small left-lateral component (Doğan and Karakas, 2013).

Eastern Turkey accommodates a highly elevated morphology due to the continental collision between stable Eurasia and the northward-migrating Arabian plate (Sengor and Yılmaz, 1981). The three main plate boundaries in eastern Turkey are the right-lateral North Anatolian Fault Zone (NAFZ), the left lateral East Anatolian Fault Zone (EAFZ) and the Bitlis-Zagros Suture Zone (Bulut et al., 2012) (Figure 5.1a). Interestingly, the 2011 Van earthquake occurred off the main plate boundary on the Bardakçı-Saray Thrust Fault Zone (BSTFZ, Figure 5.1a). The surface rupture is limited to a length of 8 km, indicating that most of the mainshock slip occurred below the surface. Therefore, the fault accommodating the 2011 Van earthquake has been interpreted to be a blind thrust fault to a large extent (Doğan and Karakas, 2013).

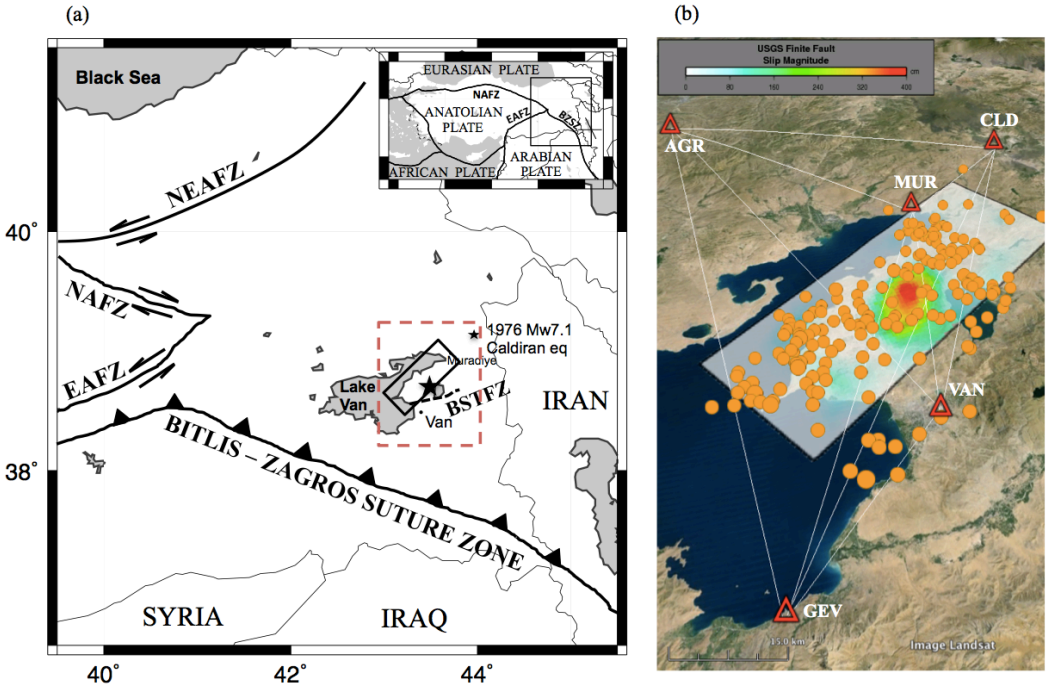

Figure 5.1. (a) Tectonic setting of the target area: North Anatolian Fault Zone (NAFZ), East Anatolian Fault Zone (EAFZ), North-East Anatolian Fault Zone (NEAFZ), Bitlis-Zagros Suture Zone, Bardakçı-Saray Thrust Fault Zone (BSTFZ). The large star indicates the hypocenter of the 2011 Van earthquake. (b) Rupture plane (projected white rectangle), co-seismic slip distribution (color-encoded with warm colors corresponding to high values reaching 4m) (both after Hayes, 2011) and M>4 aftershocks of the 2011 Van M 7.1 earthquake (yellow circles). Red triangles and white lines are broadband stations and interstation ray paths used in this study, respectively.

The aftershocks are distributed mostly outside the nucleation zone extending beneath Lake Van in the west and towards the town of Muradiye in the east, near the epicenter of the 1976 Çaldıran earthquake (M 7.1) (Figure 5.1b). The region falling between the eastern tip of the 2011 Van aftershock activity and the 1976 Çaldıran rupture zone did not host a major earthquake since 1976 therefore probably represents a highly stressed fault segment (Akıncı et al., 2012).

5.3 Data analysis

We use continuous waveform recordings of five broadband stations operated by the Kandilli Observatory and Earthquake Research Institute in Istanbul (KOERI) (stations

AGR, CLD and VAN) and the Turkish Disaster and Emergency Presidency in Ankara (AFAD) (stations GEV and MUR) (Figure 5.1b) thereby providing ten inter-station ray paths covering different parts of the mainshock rupture and the surrounding area. Only the station CLD lacks one-month data 20 days before to 10 days after the Van earthquake. Moreover, the station MUR and VAN lack data on the day of the mainshock. Prior to the pre-processing, all waveform recordings were uniformly down-sampled to 10 Hz. We follow the data pre-processing steps described in Bensen et al. (2007): Firstly, the mean, trend and instrument response are removed. In a second step, one-bit normalization is applied to the continuous data to reduce the potential contamination of the waveforms by local seismicity and to minimize the instrumental irregularities. Additionally, we eliminate ~14.000 Van aftershocks with magnitudes >1.8 as reported in the AFAD earthquake catalogue from the waveform recordings (http://www.deprem.gov.tr/sarbis/Shared/Default.aspx). This is done since aftershocks are a potential source of uncertainty for our study. Finally, we apply spectral whitening within the bandwidth of the data to balance the frequency spectrum. At this stage, we do not perform band-pass filtering to keep all available information contained in the waveform recordings. We analyze the time period of July 2011 – January 2012, thus evenly framing the 2011 Van earthquake that occurred in October 2011. A daily cross-correlation is computed by stacking non-overlapping three-minute long time windows moving along a six-month long data stream. We do not include the mainshock day.

The direct surface waves are highly sensitive to the temporal variations of internal sources, such as aftershocks (Wegler et al., 2009). In a strongly scattering medium, the coda waves repeatedly sample the same region and therefore are more sensitive to

small changes within the medium (Snieder et al., 2002; Snieder 2006). We apply the stretching technique (Sens-Schönfelder and Wegler, 2006) focusing on the coda part of the stacked cross-correlation functions to attenuate the effect of internal sources. The coda window to be used for the temporal analysis, is selected as a 60 s wide band starting ~10 s after the energy of the direct waves decrease at all five stations. We perform time domain cross-correlations on the vertical components, assuming that within the frequency band of interest the coda part of the correlations is composed of surface waves (Margerin et al., 2009; Froment et al., 2013) thus focusing on the Rayleigh-type ambient noise field.

We first calculate a mean cross-correlation function out of all daily correlations to be used as a reference trace. This reference cross-correlation is then compared with each individual/daily cross-correlation, which is further smoothened (moving window average over the following 30 days) in order to calculate corresponding time shifts (Figure 5.2a).

The method elongates the time axis of the individual correlation with a stretching parameter (by stretching or compressing) and interpolates the amplitude of this trace. The reference trace and the individual traces are then cross-correlated to measure the relation between the stretching parameter and the corresponding waveform similarity (Wegler and Sens-Schönfelder, 2006; Minato et al., 2012). A grid search algorithm is performed to find the stretching parameter providing the best-possible correlation coefficient (Figure 5.2b). The resulting stretching parameters allow to estimate the relative time shifts and therefore the corresponding velocity changes during the time period analyzed (Hadziioannou et al., 2009).

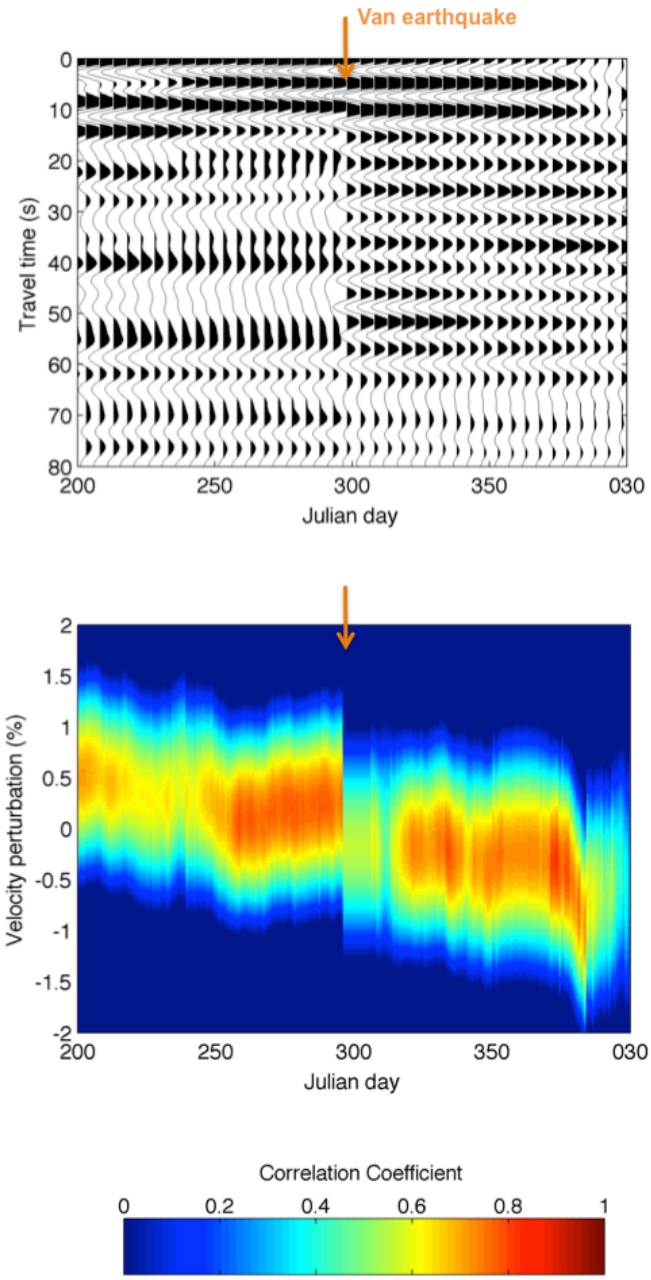

Figure 5.2. (a) Daily cross-correlations for the station pair VAN-CLD, band-pass filtered between 0.05-0.3 Hz. The orange arrow indicates the time of the 23 October, 2011, Van earthquake. The difference in the correlations before and after the earthquake is evident. (b) The velocity perturbation calculated from the time shifts by comparing each daily cross-correlation in Figure 5.2a with the corresponding reference cross-correlation and the correlation coefficient. Following the mainshock, an abrupt decrease in seismic velocity can be seen.

All ten ray paths between the station pairs are included in our analysis in order to investigate potential co-seismic velocity perturbations in the near vicinity of the

mainshock hypocenter with the best possible spatial coverage and resolution. The time shifts observed for coda waves are caused by changes within an area remaining between the stations (Wegler et al., 2009). Based on the distribution of available inter-station distances, we consider the cross-correlations within the frequency band of 0.05-0.3 Hz. The frequency band of 0.05-0.3 Hz corresponds to a wide depth range between 5 and 20 km, mixing the effects of middle and upper crust. Therefore, we further analyze the depth extent of the velocity change within three different frequency sub-bands; 0.05-0.08, 0.08-0.14 and 0.14-0.26 Hz to better interpret the changes in velocity.

5.4 Results

The most prominent feature within the 0.05-0.3 Hz frequency band is an instantaneous velocity decrease corresponding to the mainshock origin time of the Van earthquake (Figure 5.3a). As discussed earlier, we eliminate the ~14.000 Van aftershocks (M>1.8) from the continuous seismic recordings thereby excluding their influence on our results (Figure 5.3b).

We observe that the velocity drops vary depending on station pairs. In particular, the station pairs GEV-CLD (0.76 %), VAN-MUR (0.55 %), VAN-CLD (0.54 %), GEV-MUR (0.36 %) and AGR-VAN (0.35 %), all sampling the high slip area, capture an abrupt co-seismic velocity change in the range of 0.3 – 0.8 %. In contrast, station pairs AGR-MUR (0.2 %), MUR-CLD (0.1 %) and AGR-CLD (0.01 %), all with paths outside the high slip area, do not outline a major velocity change.

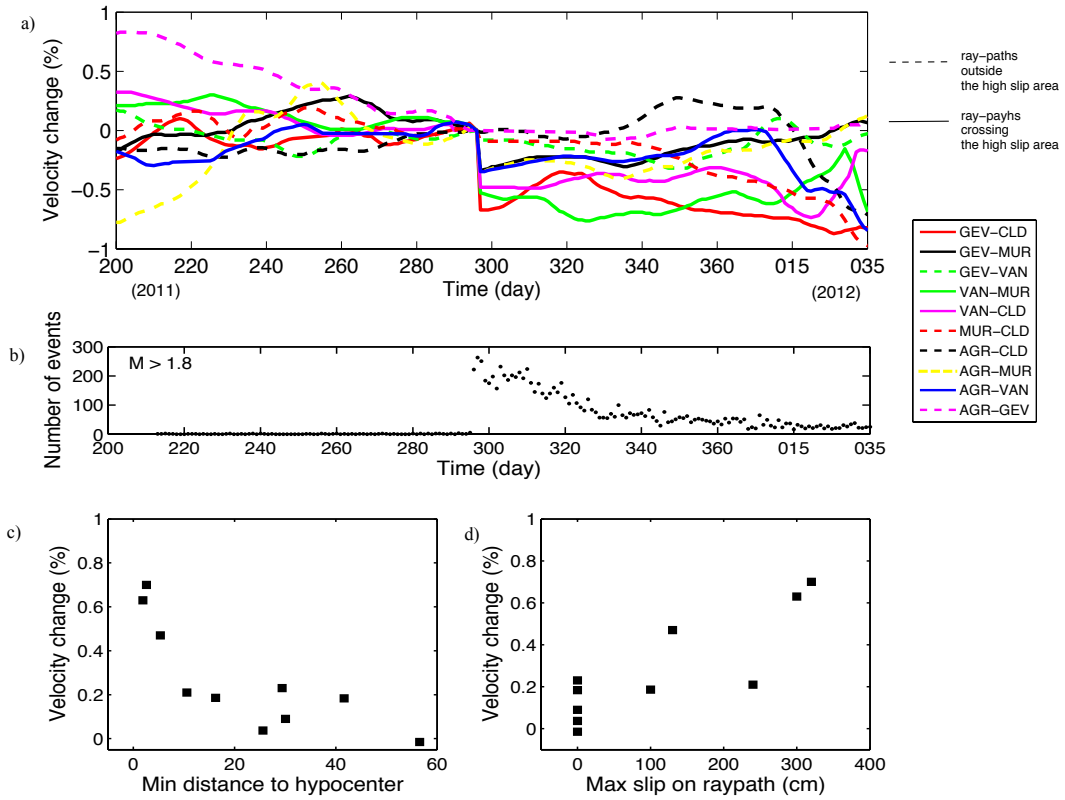

Figure 5.3 (a) Normalized velocity change with time for all ten-station pairs. Solid and dashed lines indicate station pairs with ray paths crossing and by-passing the mainshock rupture zone, respectively. (b) M>1.8 earthquakes in the Van area throughout the time period studied here. All shown events have been discarded from the waveform recordings to exclude any impact on our observations. Observed velocity change plotted with minimum distance of the respective ray path to the Van earthquake hypocenter (c) and with maximum co-seismic slip crossed by the ray paths (d), respectively.

To further elaborate on these findings, we plot the obtained co-seismic velocity change with minimum distance of the respective ray path to the mainshock hypocenter. We find that the drop in seismic velocity decreases with (the minimum) distance to the hypocenter (Figure 5.3c). Furthermore, we note that the station pairs with highest velocity changes all have ray paths passing consistently through or nearby the mainshock nucleation zone while the pairs showing small velocity changes MUR-CLD (0.1 %), AGR-CLD (0.01 %) have ray paths with relatively larger

distances to the hypocenter. Similarly, we compare the observed co-seismic velocity changes with corresponding co-seismic slip on the rupture plane. We observe that the co-seismic velocity drop scales with the maximum co-seismic slip within the crustal volume sampled by the respective ray path between the corresponding station pairs (Figure 5.3d).

The observed velocity change in the 0.08-0.14 Hz and 0.014-0.26 Hz sub-bands corresponding to relatively upper crustal layers, are almost identical (Figure 5.4b and 5.4c). Similar to the main frequency band of 0.05-0.3 Hz, we observe a drop in velocity scaling with the minimum distance of the ray path to the hypocenter. The highest velocity drops in the 0.08-0.14 Hz and 0.14-0.26 Hz sub-bands are on the order of 0.50%, observed for the station pair GEV-CLD, which represents the closest ray path to the nucleation zone. For the time period of our analysis, we observe no velocity recovery in the post-seismic stage and a steady variation in the pre-seismic stage.

Interestingly, in the sub-band of 0.05-0.08 Hz corresponding to approximately middle crustal depths (12-20 km) (Vanacore et al., 2013), there is a clear velocity increase between the station pairs with the ray paths outside the high slip area GEV-VAN (0.50 %), MUR-CLD (0.29 %), AGR-MUR (0.27 %) and AGR-GEV (0.23 %). A drop in velocity is still apparent between the station pairs crossing the high-slip area; VAN-CLD (0.54 %), GEV-CLD (0.45 %), AGR-VAN (0.22 %) and GEV-MUR (0.20 %). In addition to the velocity-change curves, the correlation coefficient (R) between the reference and daily correlation for each frequency sub-band for all ray paths is shown in Figure 5.4d as a measure for the reliability of the observations

following Wegler et al. (2009) and Hobiger et al. (2012). As it is stated in Wegler et al. (2009), a low *R* value may indicate some additional changes to the velocity change such as a variation in the distribution of noise sources. A low *R* value here refers to values below 0.5-0.6 (Wegler et al., 2009; Bulut et al., 2011). In our case the correlation coefficients (*R*) are usually well above 0.5 on average suggesting that the observed coseismic velocity changes are reliable. The velocity change curves at this long-period sub-band vary considerably in pre-and post-seismic stage compared to the short period sub-bands. Measurements performed by using the coda part of the correlations become more difficult at long periods, due to weaker scattering and slower convergence of noise correlations to empirical Green's functions (Froment et al., 2013). This may be the reason for *R* values as low as 0.4 observed in this sub-band. The variation in velocity change after the day 015 can be explained by the insufficient amount of days stacked.

In general, velocity recovery is not observed on any ray paths at short period sub-bands. However, at long periods, there is a sharp drop in velocity for the VAN-CLD ray path at the time of the mainshock but in general no stable trend is observed (Figure 5.4a). At shorter periods, there is a slight decrease in velocity before the mainshock and an immediate recovery back to almost pre-seismic values in the 0.14-0.26 Hz sub-band.

5.5 Discussion

The source area of the M 7.1 Van earthquake is characterized by a NW-dipping and NE striking rupture plane accommodating a particular patch of high co-seismic slip (up to ~ 4 m). This high-slip patch hosts only a few aftershocks and is surrounded by a larger section of reduced co-seismic slip that hosts pronounced aftershock activity.

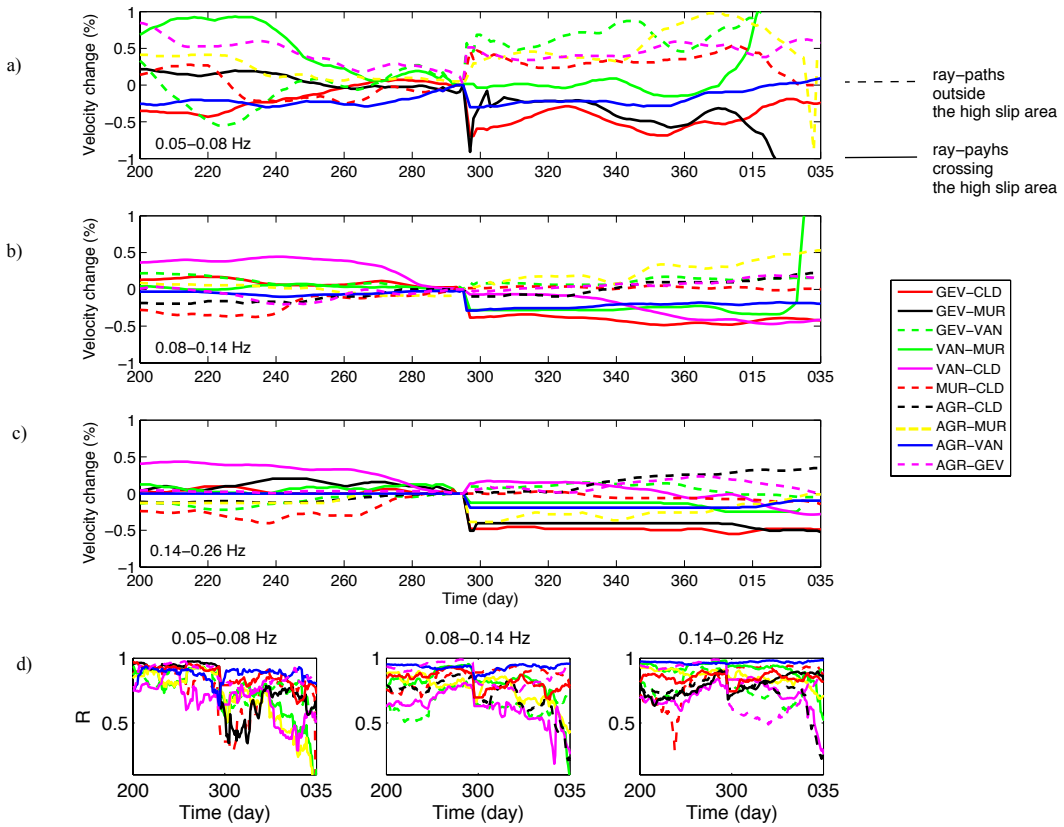

Figure 5.4. Velocity change observed at three different frequency sub-bands; a) 0.05-0.08 Hz (corresponding to upper mid-crustal depths), b) 0.08-0.14 Hz, c) 0.14-0.26 Hz. The drop in velocity within the high slip area is observed in all sub-bands. At the longer period band (a), there is an increase in velocity for the ray paths sampling the area outside the high slip zone (Figure 1b). d) Correlation coefficients (*R*) for the daily versus reference cross-correlation functions for each of the three sub-bands as a measure for the reliability of the velocity-change curves in a-c.

The slip is buried to a large extent with a centroid depth of 14 km and constrained to a depth range of 9-20 km (Elliot et al., 2013; Fielding et al., 2013). Contemporary between the highest slip patch and the patches with dense aftershocks suggests that the strain accumulated in the near vicinity of nucleation area has been completely released during the mainshock and then redistributed an immediate stress impulse to neighboring fractures/patches.

Our fundamental observation is that the 2011 Van Earthquake results in a velocity drop of up to ~0.8%. This is consistent with the previous studies indicating that major earthquakes cause a co-seismic velocity decrease within the hypocentral region (Wegler et al. (2009), Chen et al. (2010)). In principle, the amount of stress released during an earthquake (or, in other words, the strain accumulated throughout the inter-seismic period) might be on the order of >10 MPa (e.g. Oth, 2013), and is thus significantly larger than the presumable co-seismic increase in Coulomb Stress at the tips of the rupture zone (< 0.5 MPa) (e.g. King et al., 1994). We interpret this to indicate that the elastic response to an earthquake remaining within the Earth is dominated by stress release rather than relatively minor Coulomb Stress increase.

The observed velocity drop in close proximity to the mainshock hypocenter points out an impulsive elastic response of the nearby medium to a M7.1 earthquake. The main shock has activated many small-scale faults of different mechanisms within the rupture zone (Erdik et al., 2012). This response might include crack openings, fluid flow and therefore change in pore pressure deep in the crust. For shallow depths this response might be associated with near-fault damage to the source for a decrease in velocity (Rubinstein and Beroza, 2004). Our observations show a velocity change as a function of distance from the mainshock as well as a correlation between the magnitude of the velocity change and the amount of co-seismic slip. This suggests that the elastic relaxation is the highest near the hypocenter (co-seismic high-slip patch) and decreases with distance from the area most affected by the mainshock rupture.

For some station pairs (within the 0.05-0.3 Hz main frequency band), we observe a systematic recovery of the seismic velocity during the first ~80 days following the mainshock back to the pre-seismic levels (Figure 5.3a, e.g., pairs AGR-MUR, AGR-VAN, GEV-MUR). There, corresponding ray paths overlap in an area directly west of the high-slip area beneath Lake Van. One might speculate that fresh fracture networks created during the main-shock are being filled with fluids thus balancing the underground pressure (becoming same as pre-existing fluid-filled cracks) and resulting in a temporal recovery of the seismic velocity towards pre-mainshock values (King and Wood, 1994).

The driving mechanism of the 2011 Van earthquake is thrust faulting dominant at the hypocentral depths, and a small left-lateral component at the shallower parts of the fault plane (Irmak et al., 2013). This is also reflected as an increase in velocity outside the high slip area and higher magnitude of velocity change in the 0.05-0.08 Hz sub-band (corresponding to hypocentral depths) compared to the other two relatively shorter period sub-bands (Figure 5.4). The increase in the velocity diminishes with depth in correspondence with the reduced thrust component.

5.6 Conclusions

Ambient noise analysis has been successfully applied to directly measure a co-seismic change (drop) of seismic velocity in the vicinity of the M7.1 2011 Van/eastern Turkey earthquake. The broadband waveform recordings that are cross-correlated and stacked for a time period of six months framing the mainshock allow determining an average Rayleigh-wave velocity of 3.3 km/s for the target region.

The observed co-seismic velocity decrease in the hypocentral region reaches up to ~0.8 % in the frequency band of 0.05 – 0.3 Hz. The observed velocity drop is largest close to the earthquake hypocenter and decreases with distance from the mainshock rupture. A similar correlation is observed between the co-seismic velocity decrease and the amount of co-seismic slip on the part of the rupture plane penetrated by the corresponding ray paths. Within the frequency band of 0.05-0.08 Hz, corresponding to the Van hypocentral depths, an increase in velocity of about ~0.50 % is observed outside the high slip area, indicating an increase in stress level.

The observation of a drop in crustal velocity in conjunction with a M7+ earthquake shows a clear response of the brittle crust pointing out a change in elastic parameters. Such changes can be detected and even monitored with conventional regional seismic networks with inter-station spacings of several tens of kilometers and by applying available ambient noise processing techniques.

Acknowledgements

We thank the Turkish Republic Disaster and Emergency Management Presidency (AFAD Earthquake Department) and the Kandilli Observatory and Earthquake Research Institute (KOERI) for providing seismic recordings from selected seismic stations. We thank the German Research Foundation (DFG) for funding within the ICDP priority programme (grant no. Bo 1877/5-1) and the Helmholtz Foundation for funding within the Young Investigators Group: „From microseismicity to large earthquakes“.

Chapter 6

Discussion and Conclusions

The key objective of this thesis is to provide a comprehension on the structural characterization and temporal variation of seismic velocity field at different phases of the seismic cycle. Hitherto, the seismic velocity field is determined by applying traditional earthquake tomography methods to the seismic data recorded at existing networks. The precision of these tomography methods, exploiting either surface waves, full waveforms or arrival times, are bound by the density of the seismic activity and/or distribution of the receivers. In this thesis, the spatial and temporal variations of the seismic velocity field are analyzed using ambient noise field being recorded continuously at the existing networks.

Analyzing the structural variation of the seismic velocity field in the eastern Sea of Marmara, where the Princes' Islands segment of the North Anatolian Fault Zone is in the final phase of the seismic cycle, is the main focus in the first part of this study. This is performed in three steps: computing/analyzing the cross-correlations, obtaining the corresponding dispersion curves and inverting for the 1D S-wave velocity structure. The dispersion analysis of the empirical Green's functions allowed to clearly identify the basins, Çınarcık and Thrace Basins, indicated as low velocity regions due to the sedimentary fill. In this part, it is presented that ambient noise cross correlation technique is a feasible and powerful tool to image structural variations. The S-wave velocity structure obtained within this frame is further used to improve the hypocentral accuracy of 1000 local earthquakes recorded throughout the region.

The improvement in the re-calculated hypocenter locations is quantified by means of the root mean square (rms) values. The significant decrease in the rms values when using the surface-wave-derived S-wave velocity model instead of P-S-converted-wave velocity clearly shows the benefit for determining precise absolute hypocenters. The low velocity zone within 5-20 km depth range determined from the least-squares inversion of an average dispersion curve is in good agreement with the depth of observed seismic activity in the eastern Sea of Marmara region (Bulut et al., 2009). With this conclusion, it is demonstrated that a reliable S-wave velocity structure particular for the target region is an important input in further seismological approaches. These conclusions further inspires one to calculate a 3D S-wave velocity model of the target area using ambient noise field and employing more broadband stations, in order to image the upper mantle-crustal tectonic structures in more detail and improve the precision of seismic ambient noise tomography studies.

For the target area, stress measurements from the World Stress Map indicate a northwest-southeast trend for regional SH_{max} and a similar orientation is presented in other regional studies from analyzing focal mechanisms (Bohnhoff et al., 2006; Örgülü, 2011). Eken et al. (2013), by employing shear wave-splitting analysis, demonstrated that fast polarization directions show a diffuse character in the Armutlu peninsula (southern block of NAFZ) with a predominant east-west direction whereas for the northern block fast polarization directions have a northwest trending preferred orientation. These correlate well with the results that the group velocities are relatively lower for the northwest trending travel paths, between Princes' Islands and Armutlu peninsula and higher group velocities for the travel paths, between Istanbul and Kocaeli peninsula, following the trend of Princes' Islands segment which is similar to trend of regional SH_{max}.

This conclusion is a good indication that studying ambient noise can also address crustal anisotropy in case of employing more station pairs to sufficiently identify anisotropy for different azimuths. PIRES network, as mentioned briefly in Chapter 3, was installed in 2006 on the two outermost Princes' islands (Sivriada and Yassiada), to monitor the microseismic activity below the Çınarcık Basin (Bulut et al., 2009). The network consists of nine short period and one broadband stations equipped with three component sensors. These stations are deployed as two sub-arrays of five on each island (Bulut et al., 2009). In 2012, these stations are replaced with broadband seismic stations which may allow one to study radial and azimuthal anisotropy of surface waves studying the ambient noise cross correlations along the Princes' Islands segment. Moreover, by studying surface wave anisotropy one can identify the depth of the anisotropy due to the dispersive behavior of surface waves, an information difficult to obtain by shear wave splitting analysis.

The main goal in the second part of this thesis is to observe potential temporal variations of the seismic velocity field associated with a major earthquake. In order to better understand the physics of the earthquakes, a good knowledge on stress-induced changes in the crustal elastic parameters related to earthquakes or volcano evolution is crucial. The 2011 M7.1 Van earthquake occurred in a very complex tectonic setting in eastern Turkey, providing a suitable laboratory for this purpose. Once the cross correlations are calculated for a period of six months framing the mainshock, the coseismic velocity change associated with the 23 October 2011 Van earthquake is analyzed using the stretching interpolation approach (Sens-Schönfelder and Wegler, 2006). The change in velocity is presented employing the location of station pairs with respect to the high slip area. A significant decrease in the coseismic velocity, ~0.8% in the frequency band of 0.05-0.3Hz, is observed in the near vicinity of the

nucleation zone (for the ray path closest to the nucleation zone). Additionally, it is demonstrated that there exists a correlation between the coseismic velocity decrease with minimum distance of the respective ray path to the mainshock hypocenter and the amount of coseismic slip.

Cross-correlations obtained from the ambient noise recordings are analyzed in three frequency sub-bands, to better identify the depth of the mainshock-induced change in the velocity. The magnitude of the observed velocity decrease is higher in the lowest frequency band (corresponding to hypocentral depth, between 15-20km) than the two higher frequency sub-bands (corresponding to upper crustal depths), in the high-slip area. Within the same frequency band, outside the high slip area (outside the frame of the rupture zone), a velocity increase on the order of 50% is observed, an indication of an increase in the stress level.

Monitoring and identifying the change in the crustal parameters associated with an earthquake have been studied by many authors (e.g Li et al., 2003; Vidale and Li, 2003; Rubinstein and Beroza, 2004; Schaff and Beroza, 2004; Peng and Ben-Zion, 2006; Wegler and Sens-Schönfelder, 2007; Brenguier et al., 2008; Chao and Peng, 2009; Zhao and Peng, 2009; Cheng et al., 2010) and main observation is a velocity reduction. There are several mechanisms discussed to explain this mainshock-induced velocity change; opening and closure of partially fluid filled cracks by local concentration/release of shear stress (Poupinet et al., 1984; Nishimura et al., 2000; Baisch and Bokelmann, 2001), coseismic damage of rocks during dynamic rupture (Niu et al., 2008), physical damage to fault zone (Li et al., 1998; Vidale and Li, 2003; Li et al., 2003, Rubinstein et al., 2007), near surface nonlinear strong ground motion (Schaff and Beroza, 2004; Rubinstein and Beroza, 2005; Peng and Ben-Zion, 2006),

groundwater level changes (Wegler and Sens-Schönfelder, 2007), coseismic and postseismic stress change at depth (Brenguier et al., 2008).

The coseismic velocity increase observed in the middle crustal depths (lowest frequency sub-band, 0.05-0.08Hz) outside the high slip area decreases with decreasing depth as the strength of the dominant thrust component decreases. During the postseismic period stress can be recovered gradually to the preseismic stage and fluid filled cracks will then return to their original state, which results in the velocity recovery. In the main frequency band (0.05-0.3 Hz), for the ray paths overlapping in an area directly west of the high slip area beneath Lake Van, a systematic recovery of the seismic velocity to the preseismic levels is observed. The fresh fracture network created due to the mainshock, being filled with fluids and thus balancing the underground pressure may lead to a recovery of the seismic velocity to the pre-mainshock state. In this study, the temporal change in seismic velocity can be better explained by a coseismic stress change at depth rather than a near surface damage taking into account the frequency band of interest. To be able to perform long term postseismic monitoring of 2011 Van earthquake at different frequency sub-bands, more data are available to be cross-correlated which could not be done within the time frame of this study. Moreover, a future study on the variation of anisotropy associated with a major earthquake may provide more insight into the change in stress field at different depths due to employment of dispersive surface waves.

APPENDIX A

Co-seismic velocity change associated with the 2011 Van Earthquake (M7.1): Crustal response to a major event (II)

This chapter comprises the additional analysis performed for monitoring the change in seismic velocity associated with the 2011 M7.1 Van earthquake. The target area, network and pre-processing steps applied in this part of the analysis are described in detail in Chapter 3 and 5, respectively.

Besides calculating the cross correlations between the stations, autocorrelations of each station can be calculated and analyzed in order to monitor any potential velocity changes (Wegler and Schönfelder, 2007; Minato et al., 2012). In this part, the only difference is in the pre-processing steps. The autocorrelation is performed on 30 second long data segments and similarly later part of the auto correlation functions is considered for monitoring purpose.

In Figure A1a, the cross correlation functions between the stations AGR and GEV before and after the mainshock and in Figure A1b and A1c, auto correlation functions calculated for stations MUR and AGR before and after the earthquake are presented. The impact of the mainshock on data recordings can be visualized by comparing the auto/cross-correlations of/between stations.

Following the data pre-processing steps applied as described in Chapter 5, the autocorrelations are analyzed in three frequency bands: 0.05-0.08Hz, 0.08-0.14Hz and 0.14-0.26Hz. The results are presented in Figures A2-A7. In general, the coseismic

change in velocity is almost identical for all the stations within the higher frequency bands 0.08-0.14Hz and 0.14-0.26Hz.

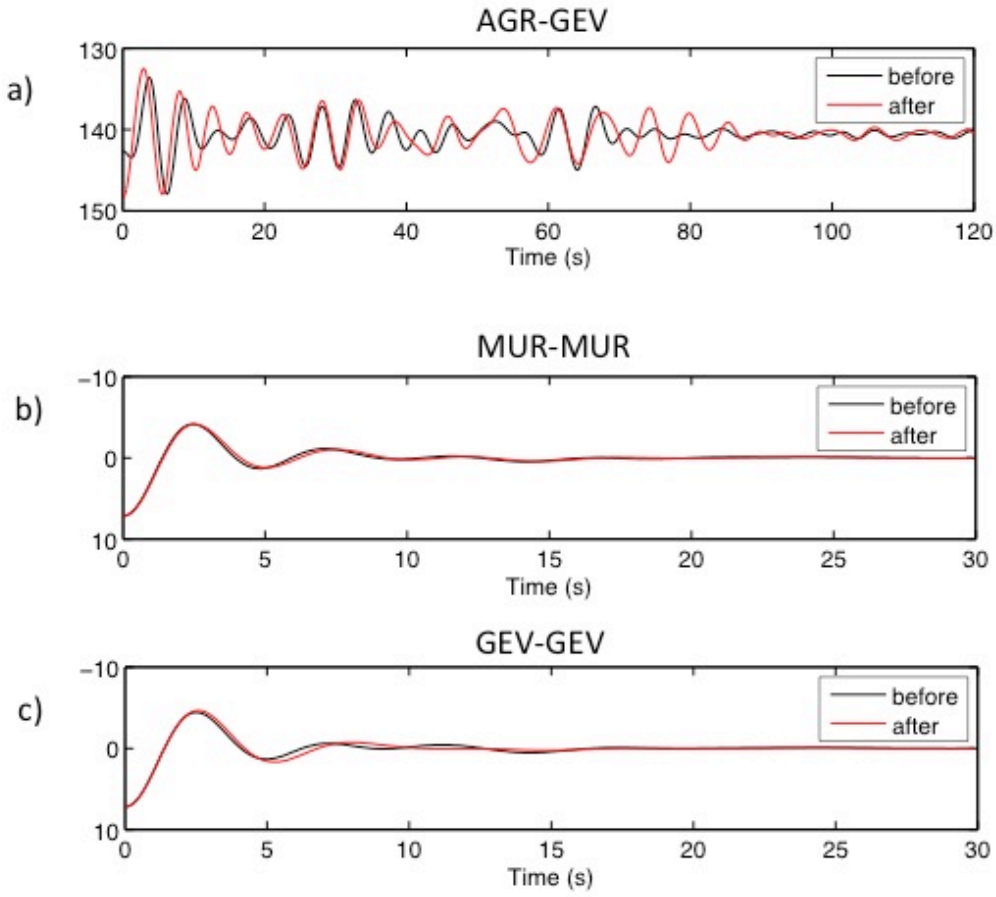

Figure A1. a) The cross-correlation function band-pass filtered in 0.05-0.3 Hz range before (in black bold line) and after (red bold line) the 2011 Van earthquake between the stations AGR and GEV. b) and c) The auto-correlation functions of stations MUR and GEV, respectively, for three-month stack before (black) and three-month stack of the auto correlation functions after the main event (red).

A velocity increase is only observed within the frequency band of 0.05-0.08 Hz for the stations GEV and AGR, which are located outside the high-slip area. Interestingly, within the 0.08-0.14Hz band, for station VAN, an increase of ~0.9 % in velocity is observed.

In Figure A8, the coulomb stress change (in MPa) maps for several depth slices (5, 10, 15, 20 km) are presented (Elliott et al., 2013). The authors calculated the coulomb stress change by using the USGS Coulomb 3.1 software and prepared these maps by assuming two uniform slipping segments with the following average reverse faulting values; strike angle of 254°, rake 83° and a dip angle of 48°.

At the depth slices of 15 to 5 km as seen in Figure A7a-b-c, the station VAN is located in an area of stress load where an increase in velocity can be observed. Moreover, this station is located in close proximity to the hypocenter of the M5.7 9 November 2011 event.

Within the rupture area (framed by the yellow box) aftershocks are focused; stress release and high slip rates therefore decrease in velocity can be observed. In the low frequency band, corresponding to mid-crustal depths, the change in velocity for station VAN and CLD are not stable enough to make a reliable statement. In station MUR, no variation in seismic velocity associated with the mainshock is observed for three frequency bands. In the higher frequency bands, either a decrease in velocity or no change is observed. Taking into account the frequency bands of interest, observed coseismic velocity change is mainly a result of stress change at depth supporting the conclusion in Chapter 5.

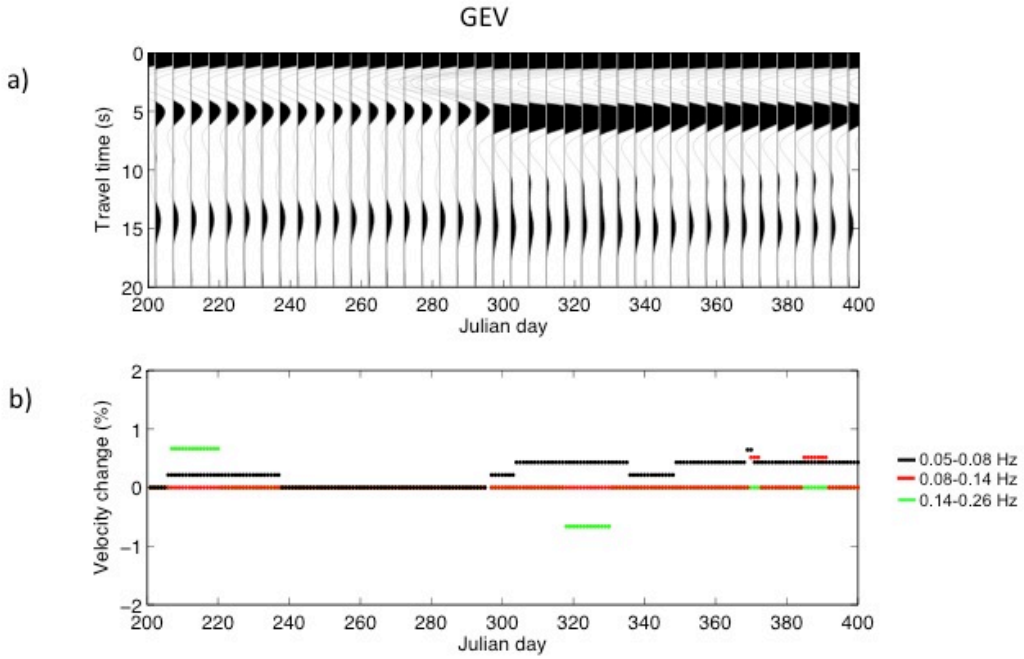

Figure A2. a) Auto correlation function of station GEV in the frequency band 0.05-0.3 Hz for the six-month period framing the main shock. b) Corresponding velocity change observed at three different frequency bands; 0.05-0.08 Hz (black dots), 0.08-0.14 Hz (red dots) and 0.14-0.26 Hz (green dots).

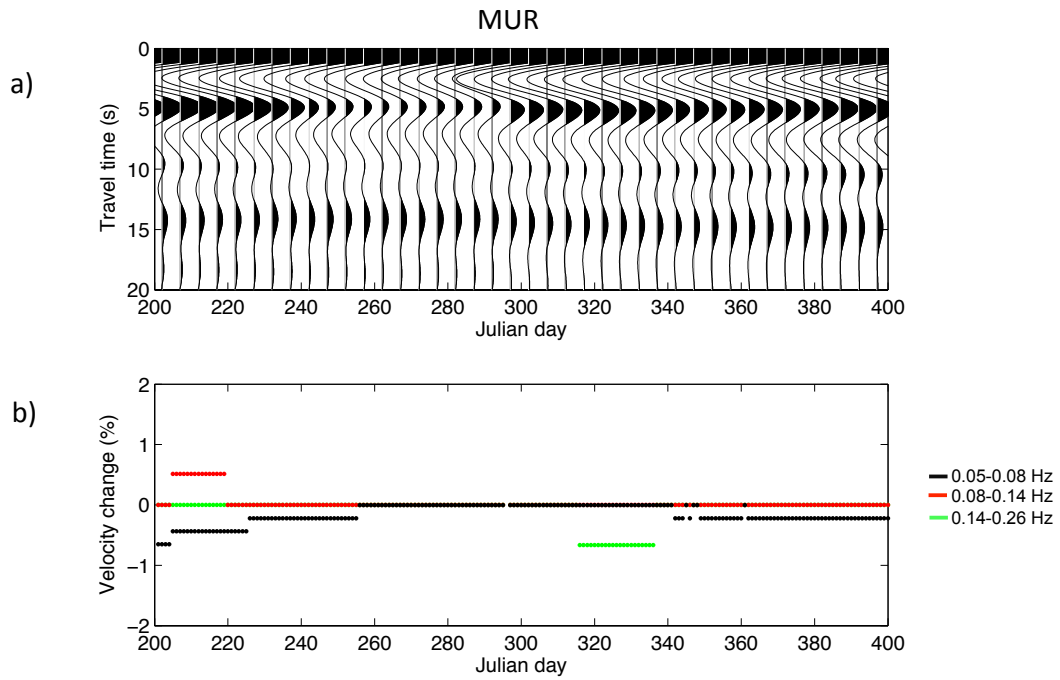

Figure A3. Same as Figure A2 but for station MUR.

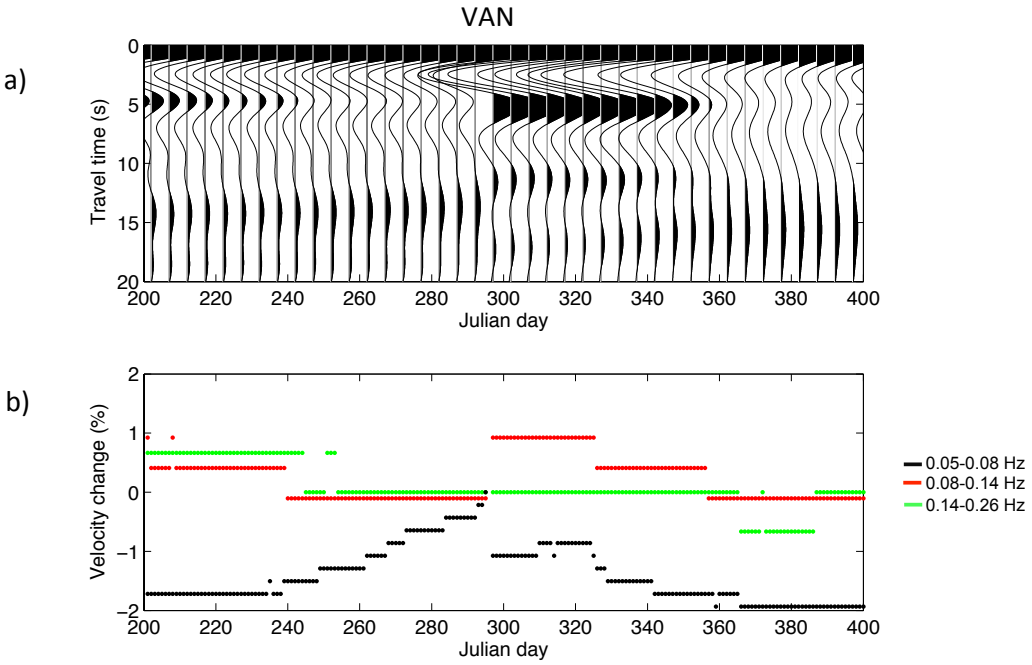

Figure A4. Same as Figure A2 but for station VAN.

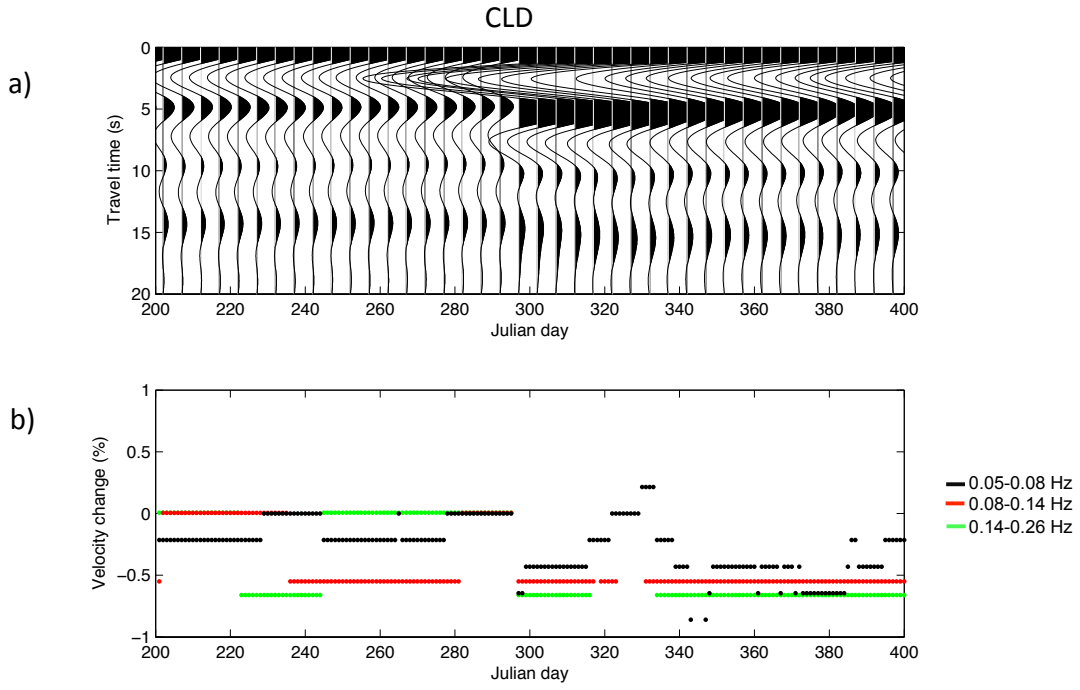

Figure A5. Same as Figure A2 but for station CLD.

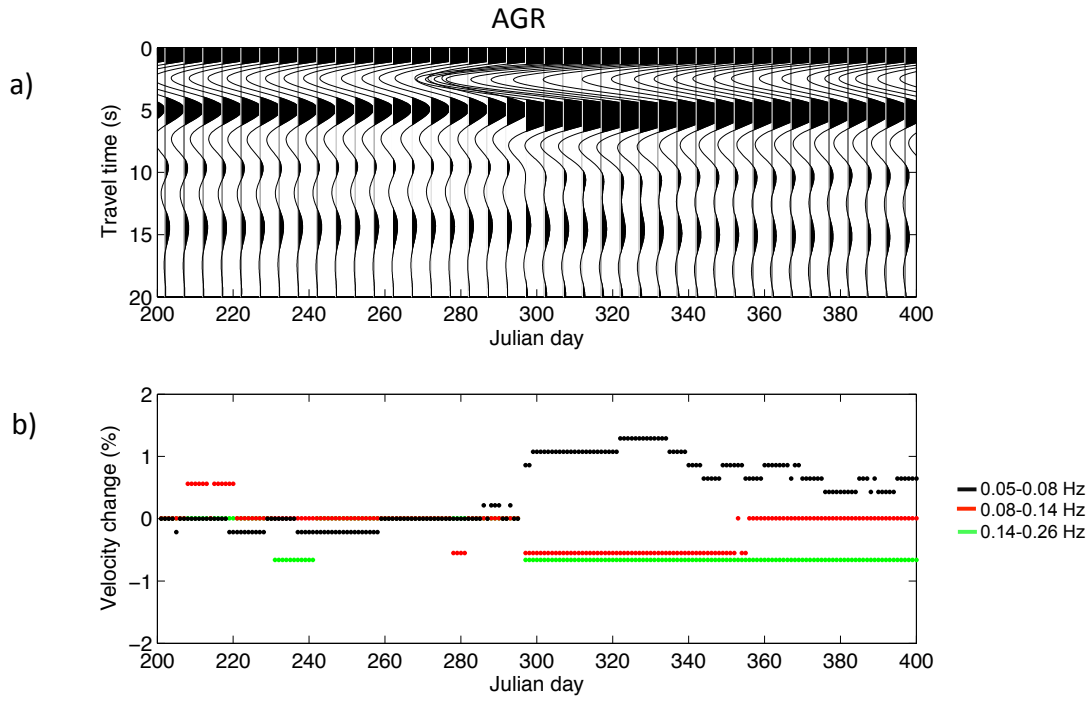

Figure A6. Same as Figure A2 but for station AGR.

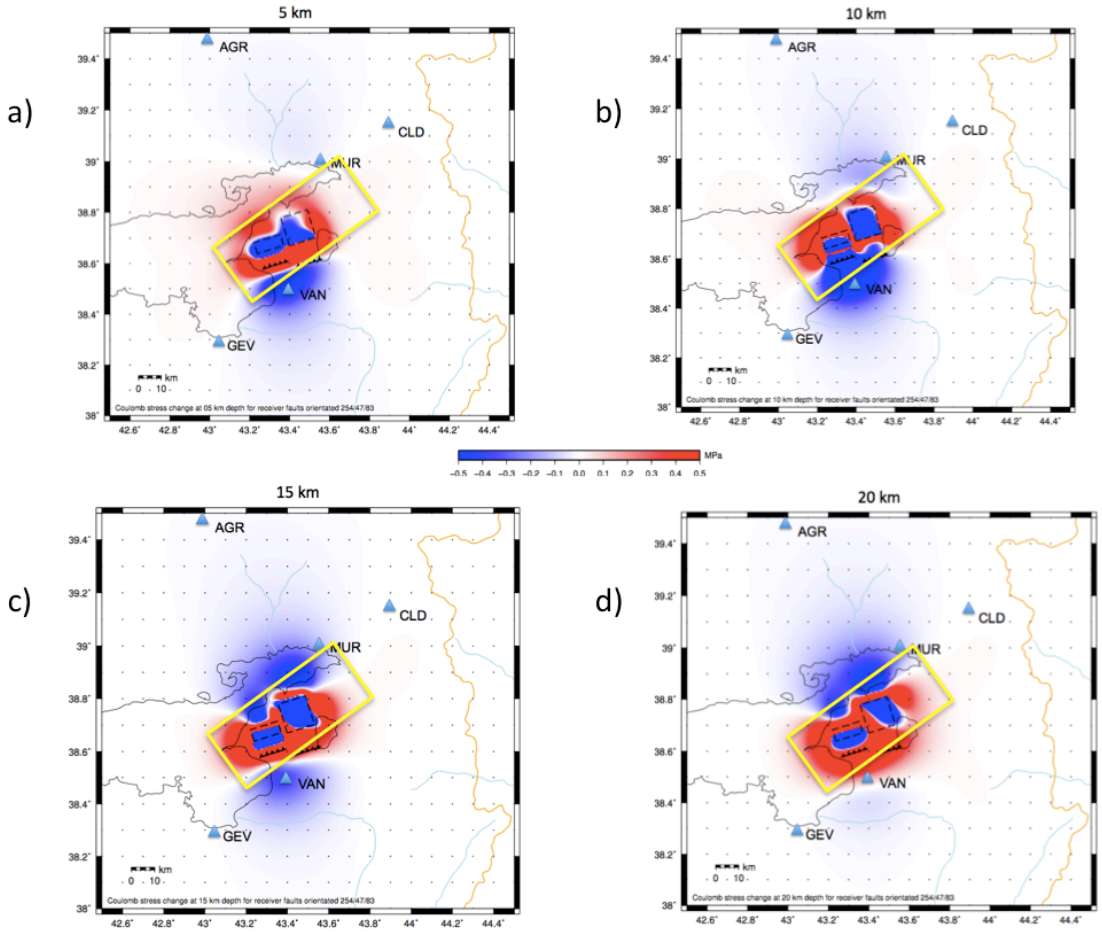

Figure A7. Coulomb stress change (in MPa) maps at depths of a) 5km, b) 10km c) 15km and d) 20 km (Elliott et al., 2013). The stations used in this study are indicated by blue triangles. The yellow rectangle frames the projection of the surface rupture. Fault friction of 0.4, Young modulus of 8e10 Pa with a Poisson ratio of 0.25 are used during calculations.

APPENDIX B

This section comprises the detailed outcome of the analysis performed in Chapter 5, as presented in Figure 5.2 but for all station pairs, at three frequency bands of interest. The results of this analysis, shown in Figures B1-B5, constitute the velocity change curves presented in Figure 5.4.

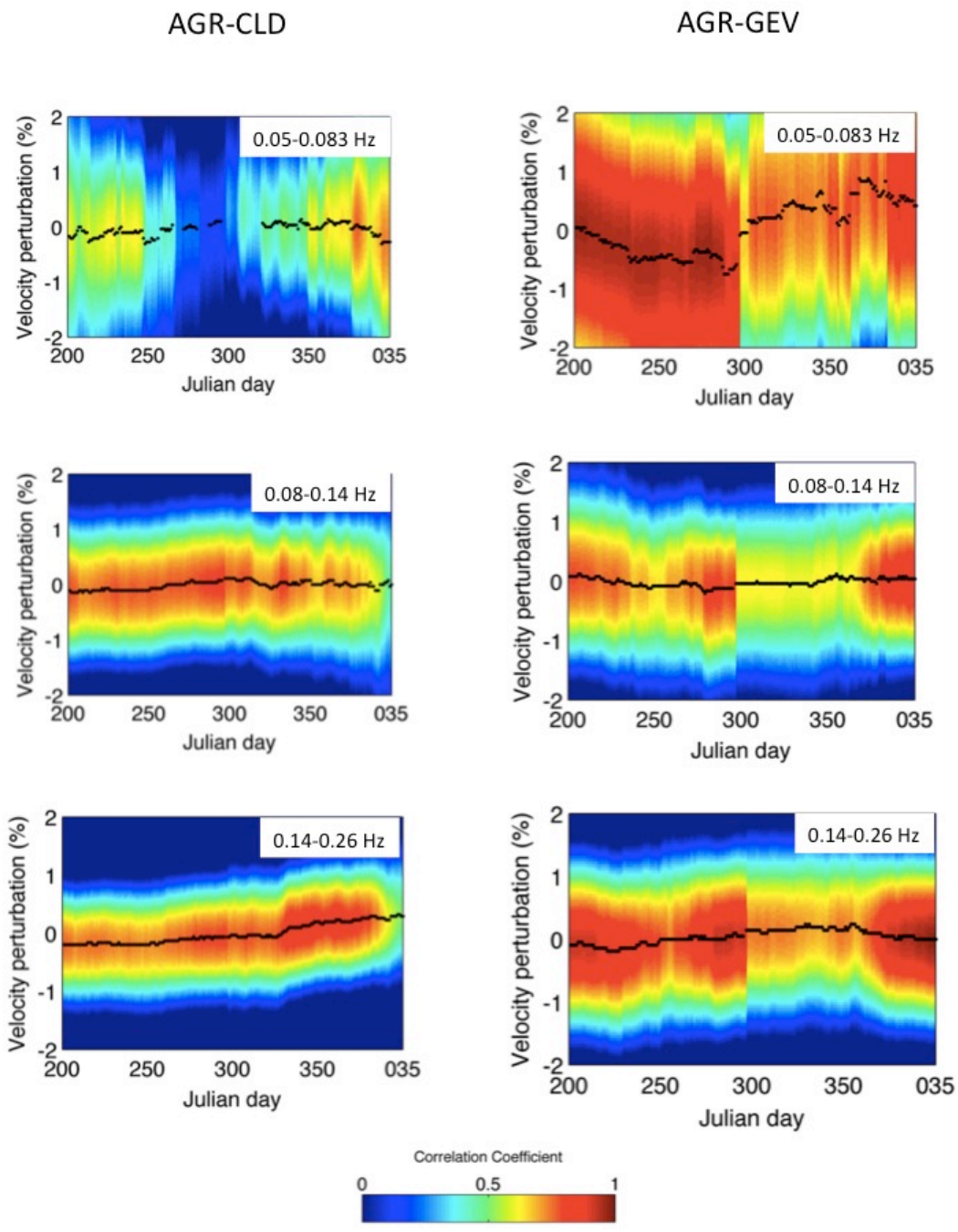

Figure B1. The velocity perturbation calculated from the time shifts by comparing each daily cross-correlation with the corresponding reference cross-correlation and the correlation coefficient for station pairs AGR-CLD (left panel) and AGR-GEV (right panel) at three different frequency bands (0.05-0.08Hz, 0.08-0.14Hz and 0.14-0.26Hz)

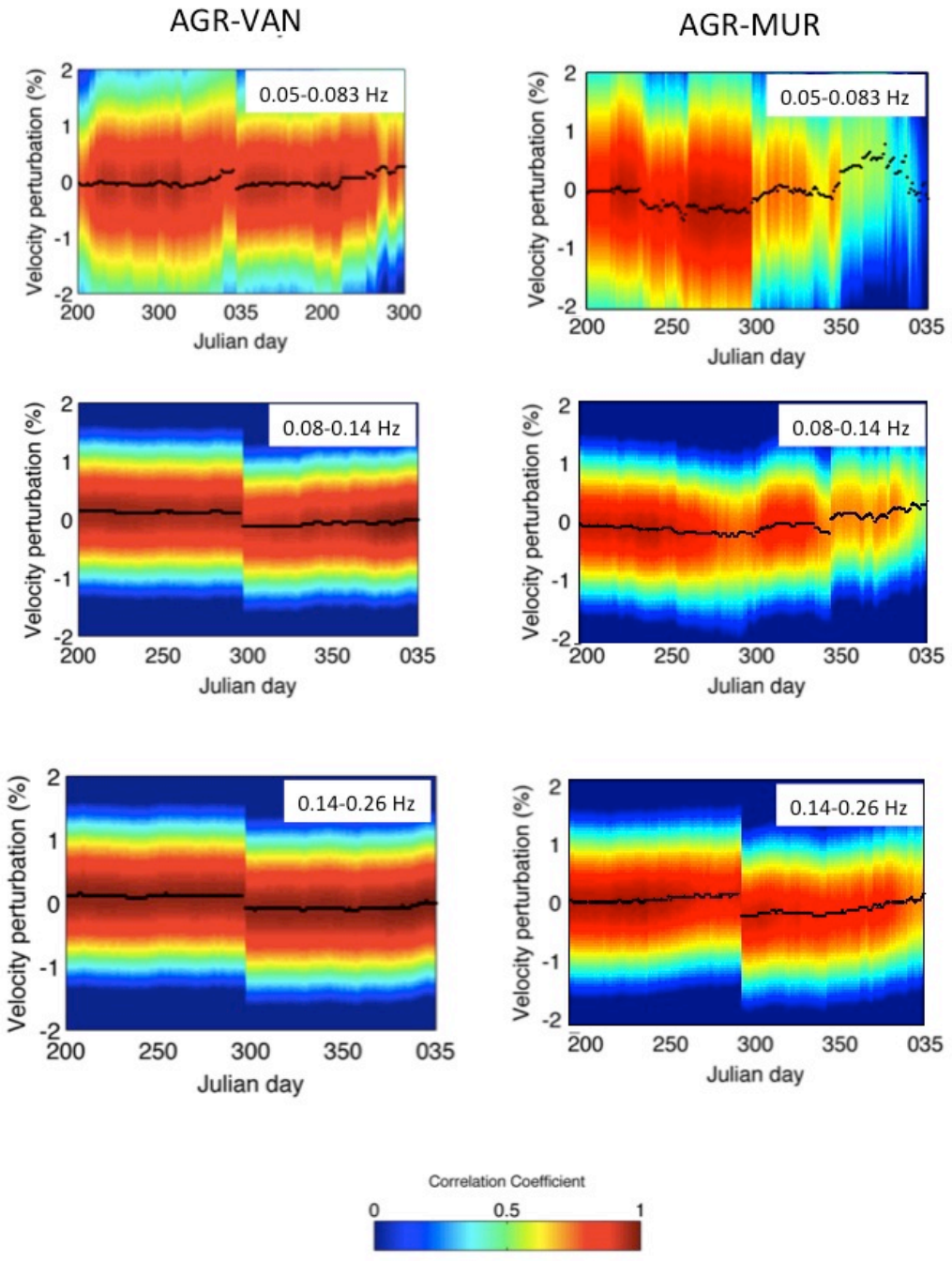

Figure B2. Same as Figure B1 for station pairs AGR-VAN and AGR-MUR.

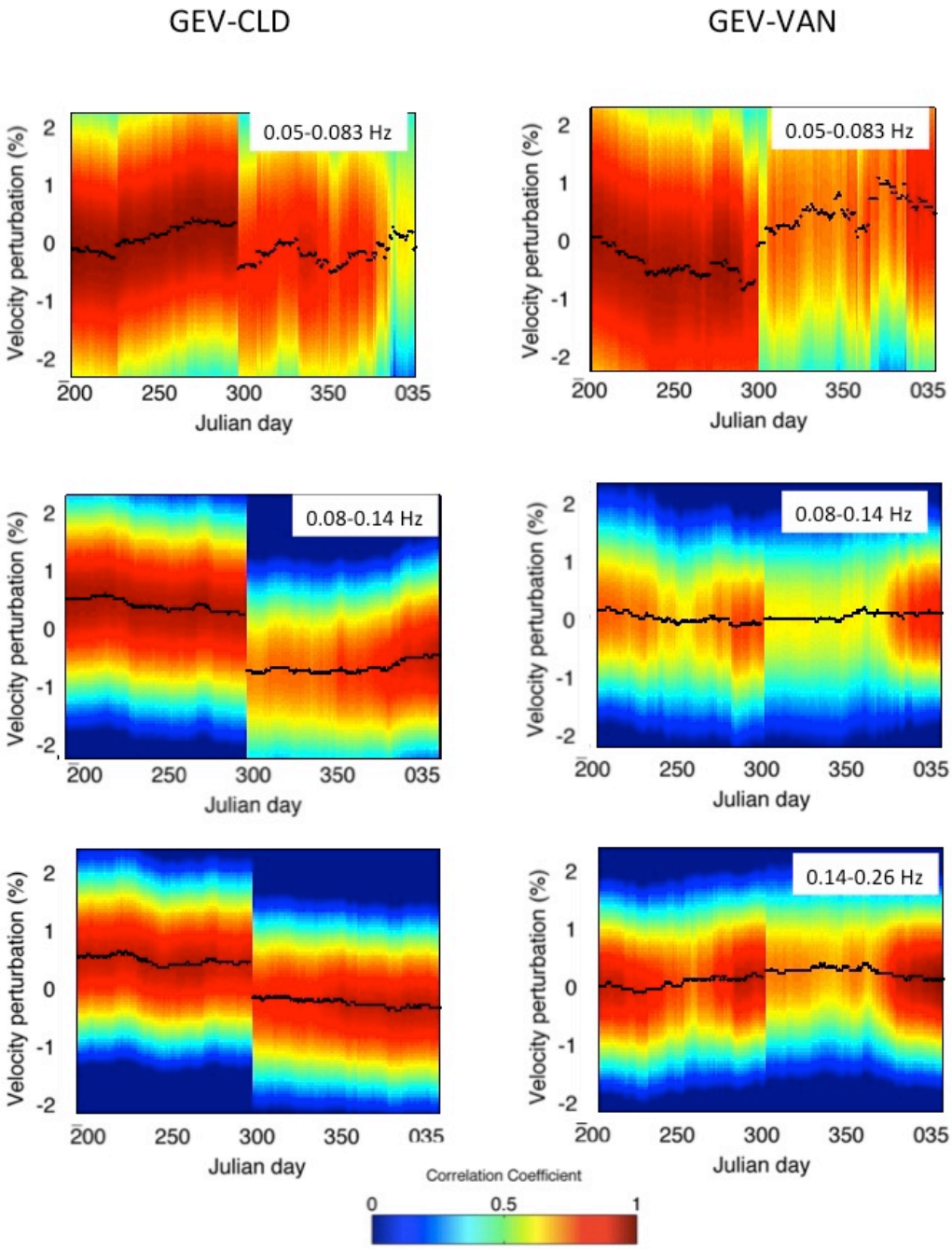

Figure B3. Same as Figure B1 for station pairs GEV-CLD and GEV-VAN.

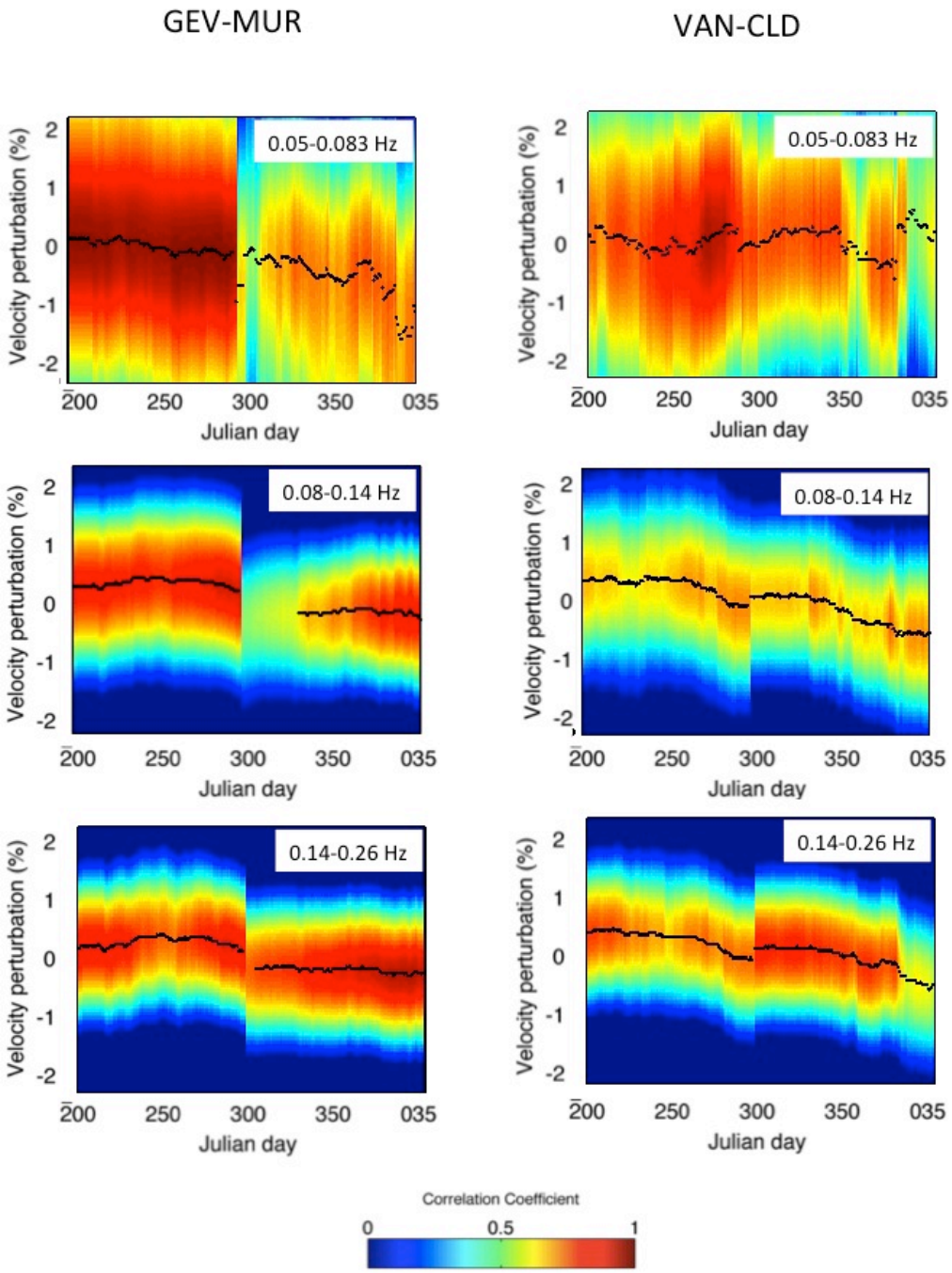

Figure B4. Same as Figure B1 for station pairs GEV-MUR and VAN-CLD.

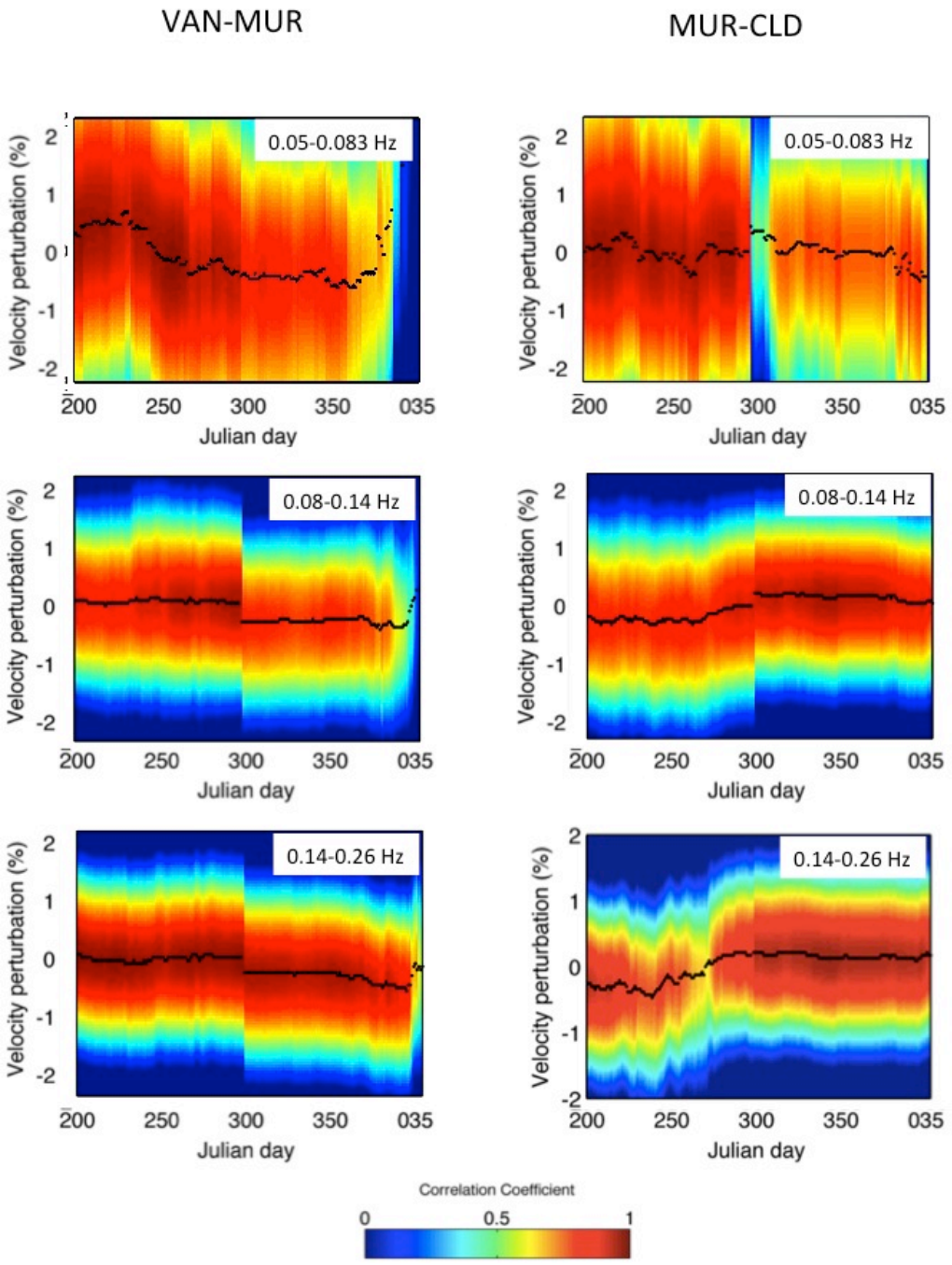

Figure B5. Same as Figure B1 for station pairs VAN-MUR and MUR-CLD.

References

Akıncı, A. and A., Antonioli, (2012). Observations and stochastic modeling of strong ground motions for the 2011 October 23 Mw 7.1 Van, Turkey, earthquake, *Geophys. J. Int.*, doi: 10.1093/gji/ggs075.

Aki, K., (1957). Space and time spectra of stationary stochastic waves with special reference to microtremors, *Bull. Earthquake Res. Inst. Tokyo Univ*., **35**, 415-457.

Aki, K., (1965). A note on the use of microseisms in determining the shallow structures of the earth's crust. *Geophysics* **30** (4), 665–666.

Aki, K., (1985). Theory of earthquake prediction with special reference to monitoring of the quality factor of lithosphere by the coda method, *Earthquake Predict. Res*., **3**, 219-230.

Ambraseys, N.N., (1970). Some characteristic features of the North Anatolian fault zone into the north Aegean. *Tectonophysics*, **9**, 143-165.

Ambraseys, N.N., (1989). Temporary seismic quiescence: SE Turkey, *Geophys. J.,* **96**, 311–331.

Al-Lazki, A., D. Seber, E. Sandvol. N. Türkelli, R. Mohamad and M. Barazangi, (2003). Tomographic Pn velocity and anisotropy structure beneath the Anatolian plateau (eastern Turkey) and the surrounding regions, *Geophys. Res. Lett*., 30(24).

Armijo R., Meyer B., Navarro S., King G. and A. Barka, (2002). Asymmetric slip partitioning in the Sea of Marmara pull-apart: a clue to propagation processes of the North Anatolian Fault*, Terra Nova* **14** (2), 80-86.

Asten, M.W., (1978). Geological control of the three-component spectra of Rayleigh-wave microseisms, *Bull. Seism. Soc. Am*. **68** (6), 1623–1636.

Asten, M.W. and J.D. Henstridge, (1984). Arrays estimators and the use of microseisms for reconnaissance of sedimentary basins, *Geophysics,* **49** (11), 1828–1837.

Asten, M.W., (2006). On bias and noise in passive seismic data from finite circular array data processed using SPAC methods, *Geophysics*, **71**(6), V153-V162. doi: 10.1190/1.2345054

Ateş, A., T. Kayıran, and I. Sincer, (2003). Structural interpretation of the Marmara region, NW Turkey, from aeromagnetic, seismic and gravity data, *Tectonophysics* **367**, Issues 1–2, 2, Pages 41–99.

Baisch, S. and G.H.R. Bokelman, (2001). Seismic waveform attributes before and after Loma Prieta earthquake: Scattering change near the earthquake and temporal recovery, *J. Geophys. Res*., **106**, No. B8, Pages 16,323-16,337.

Barka, A., (1992). The North Anatolian Fault, *Ann. Tectonicae*, **6,** 164-195.

Barka, A., (1999). The 17 August Izmit earthquake, *Science*, **285**, 1858-1859.

Barka, A. and 21 others, (2002). The Surface Rupture and Slip Distribution of the 17 August 1999 Izmit Earthquake (M 7.4), North Anatolian Fault. *Bull. Seism. Soc. Am.*, 92(1), 43-60.

Bensen, G. D., M. H. Ritzwoller, M. P. Barmin, A. L. Levshin, F. Lin, M. P. Moschetti, N. M. Shapiro, and Y. Yang, (2007). Processing seismic ambient noise data to obtain reliable broad-band surface wave dispersion measurements, *Geophys. J. Int.* **169**, 1239–1260, doi 10.1111/j.1365-246X.2007.03374.x.

Bensen, G. D., M. H. Ritzwoller, and N. M. Shapiro, (2008). Broadband ambient noise surface wave tomography across the United States, *J. Geophys. Res*. **113**, B05306, doi:10.1029/2007JB005248.

Bettig, B., Bard, P.-Y., Scherbaum, F., Riepl, J., Cotton, F., Cornou, C., and D. Hatzfeld, (2001). Analysis of dense array noise measurements using the modified spatial auto-correlation method (SPAC) Application to the Grenoble area, *Bollettino Di Geofisica Teoricaed Applicata,* **42** (3–4), 281–304.

Beroza, G.C., A.T. Cole and W.L. Ellsworth, (1995). Stability of coda wave attenuation during the Loma Prieta, California, earthquake sequence, *J. Geophys. Res.,* **100,** 3977–3987.

Birch, F. (1966). Compressibility; elastic constants in: S.P Clark (Ed.), *Handbook of Physical Constants, Geol. Soc. Am. Memoir*, **97** (1966), 97–173.

Bird, P. (2003). An updated digital model of plate boundaries, *Geochem. Geophys. Geosyst*. **4,** no. 3, 1027, doi: 10.1029/2001GC000252.

Bohnhoff, M., H. Grosser and G. Dresen, (2006). Strain partitioning and stress rotation at the North Anatolian fault zone from aftershock focal mechanisms of the 1999 Izmit Mw=7.4 earthquake, *Geophys. J. Int*., **166**(1), 373-385.

Bohnhoff, M., F. Bulut, G. Dresen, P.E. Malin, T. Eken, and M. Aktar, (2013). An earthquake gap south of İstanbul, Nat. Commun., doi: 10.1038/ncomms2999.

Bonnefoy-Claudet, S., Cornou, C., Bard, P.-Y. and F. Cotton, (2004). Nature of noise wavefield. *SESAME report*, D13.08 (http://sesame-fp5.obs.ujf-grenoble.fr).

Bouchon, M., M.N. Toksöz, H. Karabulut, M.-P. Bouin, M. Dietrich, M. Aktar and M. Edie, (2002). Space and Time Evolution of Rupture and Faulting during the 1999 Izmit (Turkey) Earthquake, *Bull. Seism. Soc. Am.*, **92**(1), 256-266.

Brenguier, F., N.M. Shapiro, M. Campillo, A. Nercessian and V. Ferrazzini, (2007). 3-D surface wave tomography of the Piton de la Fournaise volcano using seismic noise correlation, *Geophysical Research Letters*, **34**, L02305.

Brenguier, F., M. Campillo, C. Hadziioannou, N.M. Shapiro, R.M. Nadeau and E. Larose, (2008). Postseismic relaxation along the San Andreas fault at Parkfield continuous seismological observations, *Science*, DOI: *10.1126/science.1160943*

Bulut, F. and M. Aktar, (2007). Accurate relocation of *İ*zmit earthquake (Mw = 7.4, 1999) aftershocks. *Geophys. Res. Lett.*, **34**, L10307.

Bulut, F., M. Bohnhoff, W.L. Ellsworth, M. Aktar and G. Dresen, (2009). Microseismicity at the North Anatolian Fault in the Sea of Marmara Offshore İstanbul, *J. Geophys. Res*. doi: 10.1029/2008JB006244.

Bulut F., W.L. Ellsworth, M. Bohnhoff, M. Aktar and G. Dresen, (2011). Spatiotemporal Earthquake Clusters along the North Anatolian Fault Zone Offshore İstanbul, *Bull. Seism. Soc. Am*, **101**, 1759-1768, doi: 10.1785/0120100215.

Bulut, F., Bohnhoff, M., Eken, T., Janssen, C., Kl, T. and G. Dresen, (2012). The East Anatolian Fault Zone: Seismotectonic setting and spatiotemporal characteristics of seismicity based on precise earthquake locations, *Journal of Geophysical Research B: Solid Earth*, **117** (7).

Campillo, M. and A. Paul, (2003). Long range correlations in the diffuse seismic coda, *Science*, **299**(5606), 547-549, *DOI:* 10.1126/science.1078551.

Capon J., Greenfield R.J. and R.J. Kolker, (1967). Multidimensional maximum-likelihood processing of a large aperture seismic array, *Proc. IEEE*, **55(2)**, 192–211.

Capon, J., 1969. High-resolution frequency–wavenumber spectrum analysis, *IEEE*, 1408–1419.

Carton, H., S.C Singh, A. Hirn, S. Bazin, B. de Voogd, A. Vigner, A. Ricolleau, S. Cetin, N. Ocakoglu, F. Karakoç and V. Sevilgen, (2007). Seismic imaging of the three-dimensional architecture of the Çınarcık Basin along the North Anatolian Fault, *J. Geophys. Res.* **112**, B06101, doi:10.1029/2006JB004548.

Chao, K., and Z. G. Peng, (2009). Temporal changes of seismic velocity and anisotropy in the shallow crust induced by the 1999 October 22 M6.4 Chia-Yi, Taiwan earthquake, *Geophys. J. Int*., **179**, 1800–1816. doi: 10.1111/j.1365-246X.2009.04384.x.

Chavez-Garcia F. J. and L. Quintanar, (2010). Velocity structure under the Trans-Mexican Volcanic Belt: preliminary results using correlation of noise, *Geophys. J. Int.* **183**, 1077-1086.

Chen, J. H., B. Froment, Q. Y. Liu and M. Campillo, (2010). Distribution of seismic wave speed changes associated with the 12 May 2008 Mw 7.9 Wenchuan earthquake, *Geophys. Res. Lett*., **37**, L18302, doi:10.1029/2010GL044582.

Cheng, X., (2008). Time-lapse imaging of fault properties at seismogenic depth using repeating earthquakes, active sources and seismic ambient noise, *PhD Thesis*, Rice University, Houston, Texas.

Cheng, X., F. Niu and B. Wang, (2010). Coseismic velocity change in the rupture zone of the 2008 Mw 7.9 Wenchuan earthquake observed from ambient seismic noise, *Bull. of Seism. Soc. Am*., **100**(5B), 2539-2550.

Chesnokov, E.M. and S.V. Zatsepin (1991). Effects of applied stress on effective elastic anisotropy in cracked solids, *Geophys. J. Int*., **107**(3), 563-596.

Cho, K.H., R.B. Herrmann, C.J. Ammon, and K. Lee, (2007). Imaging the Upper Crust of the Korean Peninsula by surface-wave tomography, *Bull. Seism. Soc. Am.*, **97(1)**, 198-207.

Christensen, N. and H. Wang, (1985). The influence of pore pressure and confining pressure on dynamic elastic properties of Berea sandstone, *Geophysics*, **50**(2), 207–213. doi: 10.1190/1.1441910

Claerbout, J., (1968). Synthesis of a layered medium from its acoustic transmission response. *Geophysics*, **33**, 264–269.

Claprood, M, M.W. Asten and J. Kristek, (2011). Using the SPAC Microtremor Method to Identify 2D Effects and Evaluate 1D Shear-Wave Velocity Profile in Valleys, *Bull. of Seism. Soc. Am.*, **101**(2), 826-847. doi: 10.1785/0120090232

Claprood, M and M.W. Asten, (2009). Initial results from spatially averaged coherency, frequency-wavenumber, and horizontal to vertical spectrum ratio microtremor survey methods for site hazard study at Launceston, Tasmania, *Exploration Geophysics,* **40**:1, 132-142.

Clarke, D., L. Zaccarelli, N.M. Shapiro and F. Brenguier, (2011). Assessment of resolution and accuracy of the Moving Window Cross Spectral technique for monitoring crustal temporal variations using ambient seismic noise, *Geophys. J. Int.*, **186**(2), 867-882. doi: 10.1111/j.1365-246X.2011.05074.x

Crampin S., D.C., Booth, R., Evans, S., Peacock and J.B. Fletcher, (1990). Changes in shear-wave splitting at Anza near the time of the North Palm Springs Earthquake, *J. Geophys. Res.*, **95**, 11197–11212,

Crampin, S. and S.V. Zatsepin, (1997). Modelling the compliance of crustal rock-II. Response to temporal changes before earthquakes, *Geophys. J. Int*., **129**(3), 495-506.

Derode, A., Larose, E., Campillo, M. and M. Fink, (2003). How to estimate the Green's Function of a heterogeneous medium between two passive sensors? Application to acoustic waves, *Appl. Phys. Lett.*, **83**, 3054-3056.

Doğan, B. and Karakas A., (2013). Geometry of co-seismic surface ruptures and tectonic meaning of the 23 October 2011 Mw 7.1 Van earthquake (East Anatolian Region, Turkey), *J. Struc. Geol*., **46**, 99-114.

Duvall, T. L., Jefferies, S. M., Harvey, J. W. and M. A. Pomerantz, (1993). Time distance helioseismology, *Nature*, **362**, 430–432.

Eken, T., M. Bohnhoff, F. Bulut, B. Can, and M. Aktar (2013). Crustal anisotropy in the Eastern Sea of Marmara region in NW Turkey, *Bull. Seism. Soc. Am*., **103**, 2A, 911-924.

Elliot, J. R., A. C. Copley, R. Holley, K. Scharer and B. Parsons (2013). The 2011 Mw 7.1 Van (Eastern Turkey) earthquake, *J. Geophys. Res*., **118**, 1619–1637, doi:10.1002/jgrb.50117.

Erdik, M., Y. Kamer, M. Demircoglu and K. Sesetyan (2012), 23 October 2011 Van (Turkey) earthquake, *Nat. Hazards*, **64**, 651-665.

Fielding, E.J., Lundgren, P.R., Taymaz,T., Yolsal-Çevikbilen, S. and Owen, S.E. (2013), Fault-Slip Source Models for the 2011 M7.1 Van Earthquake in Turkey from SAR Interferometry, Pixel Offset Tracking, GPS and Seismic Waveform Analysis, *Seismological Research Letters*, **84**(4), 579-593, doi:10.1785/0220120164.

Friedrich, A., F. Kruger, and K. Klinge (1998). Ocean-generated microseismic noise located with the Grafenberg array, *J. Seismol*., **2**, 47–64.

Froment B., M. Campillo, J.H. Chen and Q.Y. Liu (2013), Deformation at deoth associated with the 12 May 2008 Mw 7.9 Wenchuan earthquake from seismic ambient noise monitoring, *Geophys. Res. Lett.*, **40**, 78-82.

Gallego, A., R.M. Russo, D. Comte, I. Mocanu, R.E. Murdie, and J.C.Vandecar (2010). Seismic noise tomography in the Chile ridge subduction region, *Geophys. J. Int.* **182**, 1478-1492. doi: 10.1111/j.1365-246X.2010.04691.x

Gouedard, P., F. Stehly, F. Brenguier, M. Campillo, C. de Verdiere, E. Larose, L. Margerin, P. Roux, F.J. Sanchez-Sesma, N.M. Shapiro and R.L. Weaver, (2008). Cross-correlation of random fields: Mathematical approach and applications, *Geophysical Prospecting*, **56**, 375-393.

Gök, R., E. Sandvol, N. Türkelli, D. Seber and M. Barazangi, (2003). Sn attenuation in the Anatolian and Iranian plateaus and surrounding regions, *Geophys. Res. Lett.,* **30**(24).

Gök, R., M. Pasyanos and E. Zor, (2007). Lithospheric structure of the continent-continent collision zone: eastern Turkey, *Geophys. J. Int*., **169**, 1079-1088.

Gret, A., R. Snieder and J. Scales, (2006). Time-lapse monitoring of rock properties with coda wave interferometry, *J. Geophys. Res. (Solid Earth)*, **111**(B3), 1978-2012.

Gülen, L., A. Pınar, D. Kalafat, N. Özel, G. Horasan, M. Yılmazer and A. M. Işıkara (2002). Surface fault breaks, aftershock distribution and rupture process of the 17 August 1999 Izmit, Turkey, earthquake, *Bull. Seism. Soc. Am*., **92**(1), 230–244.

Hadziioannou, C., E. Larose, O. Coutant, P. Roux, and M. Campillo, 2009: Stability of Monitoring Weak Changes in Multiply Scattering Media with Ambient Noise Correlation: Laboratory Experiments. *J. Acoust. Soc. Am.*, **125** (6), 3688–3695.

Hayes, G., (2011), Finite Fault Model, updated result of the Oct 23, 2011 Mw 7.1 eastern Turkey earthquake. Available at last access: May 2014, http://earthquake.usgs.gov/earthquakes/eqinthenews/2011/usb0006bqc/finite_fault.php

Harmon, N., D. Forsyth, and S. Webb, (2007). Using ambient seismic noise to determine short-period phase velocities and shallow shear velocities in young oceanic lithosphere, *Bull. Seism. Soc. Am.* **97** (6), 2009-2023.

Hasselmann, K., (1963), A statistical analysis of the generation of microseisms, *Reviews of Geophysics*, (**1**)177– 210.

Haskell, N.A., (1953). The dispersion of surface waves on multilayered media, *Bull.Seis.Soc.Am.* **43**, 17-34.

Henstridge, J.D., (1979). A signal processing method for circular arrays, *Geophysics*, **44**, 179–184.

Herrmann, R.B. and C.J. Ammon, (2002). Computer Programs in Seismology, Vol. IV, St. Louis University, Missouri.

Hobiger, M., U. Wegler, K. Shiomi and H. Nakahara, (2012). Coseismic and postseismic elastic wave velocity variations caused by the 2008 Iwate-Miyagi Nairiku earthquake, *Japan. J. Geophys. Res*., 117:B09313. doi:10.1029/2012JB009402.

Horike, M., (1985). Inversion of phase velocity of long-period microtremors to the S-wave-velocity structure down to the basement in urbanized areas. *Journal of Physics of the Earth* **33**, 59–96.

Hough, S.E., Seeber L., Rovelli A., Malagnini L., DeCesare A., Selvaggi G. and A. Lerner-Lam, (1992). Ambient noise and weak motion excitation of sediment resonances: results from the Tiber Valley, Italy, *Bull. Seism. Soc. Am*., **82**, 1186–1205.

Hubert-Ferrari, A., Barka, A., Jacques, E., Nalbant, S.S., Meyer, B., Armijo, R. Traponnier, P. and G.C.P. King, (2000). Seismic hazard in the Marmara Sea following the 17 August 1999 Izmit earthquake, *Nature*, **404**, 269-273.

Irmak, T.S., B. Doğan and A. Karakas, (2012). Source mechanism of the 23 October, 2011, Van (Turkey) earthquake (Mw=7.1) and aftershocks with its tectonic implications, *Earth Planets Space*, **64**, 991-1003.

Jin, A. and K. Aki, (1986). Temporal changes in the coda Q before the Tangshan earthquake of 1976 and the Haicheng earthquake of 1975, *J. Geophys. Res*. **91**, 665-673.

Kanamori, H., and G., Fuis (1976). Variation of P-wave velocity before and after the Galway Lake earthquake (ML=5.2) and the Goat Mountain earthquake (ML=4.7) in the Mojave Desert, *Bull. Seismol. Soc. Am*., **66**, 2017-2037.

Karabulut, H., S. Özalaybey, T. Taymaz, M. Aktar, O. Selvi, and A. Kocaoğlu (2003). A Tomographic Image of the Shallow Crustal Structure in the Eastern Marmara, *Geophys. Res. Lett.* **30**, No 24, 2277.

Keskin, M., (2003). Magma generation by slab steepening and break off beneath a subduction-accretion complex: An alternative model for collision-related volcanism in Eastern Anatolia, Turkey, *Geophys. Res. Lett*., **30**, 8046.

King, G.C.P., S.S. Ross, J. Lian, (1994), Static stress changes and the triggering of earthquakes, *Bull. Seism. Soc. Am.*, **84** (3), 935-953.

King, G.C.P. and R.M. Wood, (1994), The impact of earthquakes on fluids in the crust, *Annali di Geofisica*, **37**(6), doi:10.4401/ag-4147.

Köhler, A., Ohrnberger, M., Scherbaum, F., Wathelet, M., and Cornou, C., (2007). Assesing the reliability of the modified three-component spatial autocorrelation technique, *Geophys. J. Int*., **168**, 779-796.

Kudo, K., Kanno, T., Okada, H., Özel, O., Erdik, M., Sasatini, T., Higashi, S., Takashi, M. and Yoshida, K., (2002). Site-spesific issues for ground motions during the Kocaeli Earthquake of 17 August 1999, as inferred from array observations of microtremors and aftershocks, *Bull. Seism. Soc. Am.*, **92**, 448-4655.

Kvaerna, T. and Ringdahl, F., (1986). Stability of various FK estimation techniques, Semiannual technical summary, 1 October 1985-31 March 1986, NORSAR Scientific Report, Kjeller, Norway, 1-86/87, 29-40.

Lacoss, R. T., E.J., Kelly and T. M. Nafi, (1969). Estimation of seismic noise structure using arrays, *Geophysics*, **34**, 21–38.

Larose, E., A., Derode, M., Campillo, and M., Fink, (2004). Imaging from one-bit correlations of wideband diffuse wave fields, *J. Appl. Phys*., **95**, 8393–8399, doi 10.1063/1.1739529.

Le Pichon, X., T. Taymaz, and A. M. C. Sengör, (1999). The Marmara Fault and the future Istanbul earthquake, in International Conference on the Kocaeli Earthquake, 17 August 1999, edited by M. Karaca, and D. N. Ural, 41–54, Istanbul Tech. Univ. Press House, Istanbul.

LePichon, X., and 12 others, (2001). The active Main Marmara Fault, *Earth Planet. Science Lett.*, **192**, 595- 616.

Li, Y-G., J.E. Vidale, K. Aki, F. Xu and T. Burdette, (1998). Evidence of shallow fault zone strengthening after the 1992 M7.5 Landers, California, earthquake, *Science*, **279**(5348), 217-219, doi: 10.1126/science.279.5348.217.

Li, Y. G., J. E. Vidale, S. M. Day, D. D. Oglesby and E. Cochran, (2003). Postseismic fault healing on the rupture zone of the 1999 M7.1 Hector Mine, California, earthquake, *Bull. Seismol. Soc. Am*., **93**, 854–869.

Lin, F. C., M.P. Moschetti, M. P., and M.H. Ritzwoller, (2008). Surface wave tomography of the western United States from ambient seismic noise: Rayleigh and Love wave phase velocity maps, *Geophys. J. Int.* **173**, 281-298.

Liu, H.P., Moore, D.M., Joyner, W.B., Oppenheimer, D.H., Warrick, R.E., Zhang, W., Hamilton, J.C. and L.T. Brown, (2000). Comparison of phase velocities from array measurements of Rayleigh waves associated with microtremors and results calculated from borehole shear-wave velocity profiles, *Bull. Seism. Soc. Am.,* **90**, 666-678.

Liu, Z., J. Huang, Z. Peng and J. Su, (2014). Seismic velocity changes in the epicentral region of the 2008 Wenchuan aerthquake measured from three-component ambient noise correlation techniques, *Geophys. Res. Lett.*, **41**(1), 37-42.

Lobkis, O. I., and R. L., Weaver, (2001). On the emergence of the Green's function in the correlations of a diffuse field, *J. Acoust. Soc. Am*., **110**, 3011 –3017.

Longuet-Higgins, M. S., (1950). A theory of the origin of microseisms, *Philosophical Transactions of the Royal Society*, **243**: 1 –35.

Ma, Y., R.W. Clayton, V.C., Tsai and Z. Zhan, (2013). Locating a scatterer in the active volcanic area of Southern Peru from ambient noise cross-correlation, *Geophys. J. Int*., 192(3), 1332-1341, doi: 10.1093/gji/ggs103.

Malagnini, L., Rovelli, A., Hough, S.E., Seeber, L., (1993). Site amplification estimates in the Garigliano valley, Central Italy, based on dense arrays measurements of ambient noise. *Bull. Seism. Soc. Am*., **83**(6), 1744–1755.

Margerin, L. M., M. Campillo, B.A. Van Tiggelen, and R. Hennino, (2009). Energy partition of seismic coda waves in layered media: Theory and application to Pinyon Flats Observatory, *Geophys. J. Int.*, **177**(2), 571-585.

McClusky, S. and 27 others, (2000). Global positioning system constraints on plate kinematics and dynamics in the eastern Mediterranean and Caucasus, *J. Geophys. Res.,* **105**, 5695-5719.

Minato, S., T. Tsuji, S. Ohmi, and T. Matsuoka, (2012), Monitoring seismic velocity change caused by the 2011 Tohoku-oki earthquake using ambient noise records, *Geophys. Res. Lett.*, **39**, doi:10.1029/2012GL051405.

Moschetti, M. P., M. H. Ritzwoller, and N. M. Shapiro, (2007). Surface wave tomography of the western United States from ambient seismic noise: Rayleigh wave group velocity maps, *Geochem., Geophys., Geosys*., 8, Q08010, doi:10.1029/2007GC001655.

Nicolson, H., A. Curtis, B. Baptie, and E. Galetti, (2012). Seismic interferometry and ambient noise tomography in the British Isles, *Proc. Geol. Ass*. **123**, Pages 74-86.

Nishimura, T., N. Uchida, H. Sato, M. Ohtake, S. Tanaka, and H. Hamaguchi, (2000). Temporal changes of the crustal structure associated with the M6.1 earthquake on September 3, 1998 and the volcanic activity of mount Iwate, Japan, *Geophys. Res. Lett.,* **27**(2), 269–272.

Nishimura, T., S. Tanaka, T. Yamawaki, H. Yamamoto, T. Sano, M. Sato, H. Nakahara, N. Uchida, S. Hori and H. Sato, (2005). Temporal changes in seismic velocity of the crust around Iwate volcano, Japan, as inferred from analyses of repeated active seismic experiment data from 1998 to 2003*, Earth Planets Space,* **57***,* 41–505.

Nur, A., and G., Simmons, (1969). Stress-induced velocity anisotropy in rock: An experimental study, *Journal of Geophysical Research*, **74**(27).

Ohori, M., Nobata, A. and Wakamatsu, K., (2002). A comparison of ESAC and FK methods of estimating phase velocity using arbitrarily shaped microtremor arrays. *Bull. Seism. Soc. Am.*, **92**, 2323–2332.

Okay, A.I. and O. Tüysüz, (1999). Tethyan sutures of northern Turkey, *The Mediterranean Basins; Tertiary Extension within the Alpine Orogeny*, **156**, 475–515, Geological Society Special Publications.

Oth, A., (2013), On the characteristics of earthquake stress release variations in Japan, *Earth Planet. Sci. Lett*., 377-378, 132-141, doi : 10.1016/j.epsl.2013.06.037

Örgülü G., M. Aktar, N. Türkelli, E. Sandvol and M. Barazangi, (2003). Contribution to the seismotectonics of eastern Turkey from moderate to small sized events, *Geophys. Res. Lett*., **30**(24):8040. doi:10.1029/2003GL018258

Örgülü, G., (2011). Seismicity and source parameters for small-scale earthquakes along the splays of the North Anatolian Fault (NAF) in the Marmara Sea, *Geophys. J. Int.,* **184**(1), 385-404.

Özalaybey, S., M. Ergin, M. Aktar, C. Tapirdamaz, F. Bicman and A. Yörük, (2002). The 1999 Izmit Earthquake Sequence in Turkey: Seismological and Tectonic Aspects. *Bull. Seism. Soc. Am.*, **92**(1), 376-386.

Pandolfi, D., Bean, C.J., and G., Saccorotti, (2006). Coda wave interferometric detection of seismic velocity changes associated with the 1999 M=3.6 event t Mt. Vesuvius, *Geophy. Res. Lett*., **33**(6), doi: 10.1029/2005GL025355

Parsons, T., (2004). Recalculated probability of M7 earthquakes beneath the Sea of Marmara, Turkey, *J. Geophys. Res.* **109**,B05304,doi:10.1029/2003JB002667.

Parsons, T., S. Toda, R.S. Stein, A. Barka and J.H. Dieterich, (2000). Heightened Odds of Large Earthquakes Near Istanbul: An interaction-Based Probability Calculation, *Science*, **288**, 661-664.

Pasyanos M. E. and R.W. Walter, (2002). Crust and upper-mantle structure of North Africa, Europe and the Middle East from inversion of surface waves, *Geophys. J. Int*., **149**, 463-481.

Paul, A., Campillo, M., Margerin, L., and E. Larose, (2005). Empirical synthesis of time-asymmetrical Green functions from the correlation of coda waves, *J. Geophys. Res*., **110**, doi:10.1029/2004JB003521.

Peng Z.G. and Y. Ben-Zion, (2005). Spatio-temporal variations of crustal anisotropy from similar events in aftershocks of the 1999 M7.4 Izmit and M7.1 Düzce, Turkey, earthquake sequences, *Geophys. J. Int*., **160**, 1027–1043.

Peng, Z.G. and Y. Ben-Zion (2006). Temporal changes of shallow seismic velocity around the Karadere-Düzce branch of the North Anatolian fault and strong ground

motion, *Pure Appl. Geophys*. **163**, 567–600, doi: 10.1007/s00024-005-0034-6.

Poli, P., M. Campillo, H., Pedersen and LAPNET working group, (2012). Body-wave imaging of Earth's mantle discontinuities from ambient seismic noise, *Science*, **338**(6110), 1063-1065.

Poupinet, G., W. L. Ellsworth, and J. Frechet, (1984). Monitoring velocity variations in the crust using earthquake doublets: an application to the Calaveras fault, California, *J. Geophys. Res*., **89**(B7), 5719–5731.

Prieto, A. G., Denolle, M., Lawrence, J. F. and Beroza, G. C., 2011. On amplitude information carried by the ambient seismic field, submitted to Imaging and Monitoring with Seismic Noise.

Reilinger, R.E. and 12 others, (2000). Coseismic and Postseismic Fault Slip for the 17 August 1999, M=7.5, Izmit, Turkey Earthquake, *Science*, **289**, 1519-1524.

Renalier F., D. Jongmans, M. Campillo and P.-Y. Bard, (2010). Shear wave velocity imaging of the Avignonet landslide (France) using ambient noise cross correlation, *J. Geophys. Res.*, **15**, F03032doi:10.1029/2009JF001538.

Ritzwoller M.H. and A. Levshin, (2012). Eurasian surface wave tomography: group velocities, *J.of Geophys. Res*., **102**(B3), 4839-4878.

Rivet, D., M. Campillo, N. M. Shapiro, V. Cruz-Atienza, M. Radiguet, N. Cotte and V. Kostoglodov, (2011). Seismic evidence of nonlinear crustal deformation during a large slow slip event in Mexico, *Geophys. Res. Lett*., **38**, doi: 10.1029/2011GL047151.

Roux, P. and W. A. Kupperman, (2005). Time reversal of ocean noise. *J. Acoust. Soc. Am*., **300**, 131–136.

Roux, P., K. G. Sabra, W. A. Kuperman, and A. Roux, (2005). Ambient noise cross correlation in free space: Theoretical approach, *J. Acoust. Soc. Am*., **117**(1), 79–84, doi:10.1121/1.1830673.

Rubinstein, J. L., and G. C. Beroza, (2004). Evidence for widespread non- linear strong ground motion in the Mw 6.9 Loma Prieta earthquake, *Bull. Seismol. Soc. Am.*, **94**(5), 1595–1608.

Rubinstein, J. L., N. Uchida, and G. C. Beroza (2007). Seismic velocity reductions caused by the 2003 Tokachi-Oki earthquake, *J. Geophys. Res*., **112**, B05315, doi 10.1029/2006JB004440.

Sabra, K., Gerstoft, P., Roux, P., Kuperman, W.A., and M.C. Fehler, (2005). Extracting time- domain Green's function estimates from ambient seismic noise. *Geophysical Research Letters,* **32** (3), 1–5.

Sabra, K., Gerstoft, P., Roux, P., Kuperman, W.A., and M.C. Fehler, (2005). Surface wave tomography from microseisms in Southern California. *Geophysical Research Letters,* **32**, L14311.

Saccorotti G., Almendros J., Carmona E., Ibáñez J.M., and E. Del Pezzo, (2001). Slowness anomalies from two dense seismic arrays at Deception Island Volcano, Antarctica, *Bull. Seism. Soc. Am*., **91**, 561–571.

Sakınç , M., C. Yaltırak, F.Y. Oktay, (1999). Palaeogeographical evolution of the Thrace Neogene Basin and the Tethys–Paratethys relations at northwestern Turkey (Thrace), *Palaeogeography, Palaeoclimatology, Palaeoecology* **153**, 17-40.

Sanchez-Sesma, F.J., J.A. Perez-Ruiz, M. Campillo, and F. Luzon (2006). Elastodynamic 2D Green's function retrieval from cross-correlation: Canonical inclusion problem, *Geophys. Res. Lett.*, **33**, L13305, doi:10.1029/2006GL026454.

Savage, M.K., F.-C. Lin and J., Townend, (2013). Ambient noise cross-correlation observations of fundamental and higher-mode Rayleigh wave propagation governed by basement resonance, *Geophys. Res. Lett*., **40**(14), 3556-3561.

Sawazaki K., Sato, H., Nakahara, H., and T., Nishimura (2009). Time-lapse changes of seismic velocity in the shallow ground caused by strong ground motion shock of the 2000 western-Tottori earthquake, Japan, as revealed from coda deconvolution analysis, *Bull. of Seism. Soc. of Am*., **99**(1), 32-366.

Saygin E. and B. Kennett, (2010). Ambient seismic tomography of Australian continent, *Tectonophysics*, **481**, 116–125.

Schaff, D. P., G. C. Beroza and B. E. Shaw (1998). Postseismic response of repeating aftershocks, *Geophys. Res. Lett*., **25**, 4549–4552, doi:10.1029/ 1998GL900192.

Schaff D. P. and G. C. Beroza, (2004). Coseismic and postseismic velocity changes measured by repeating earthquakes, *J. Geophys. Res*., **109**, doi: 10.1029/2004JB003011.

Scherbaum F., Hinzen K.-G. and M. Ohrnberger, (2003). Determination of shallow shear-wave velocity profiles in Cologne, Germany area using ambient vibrations, *Geophys. J. Int*., **152**, 597–612.

Scholz, C.H., (1968). Experimental study of the fracturing process in brittle rock, *Journal of Geophysical Research*, **73**(4), 1447-1454.

Sens-Schönfelder, C. and U. Wegler, (2006). Passive image interferometry and seasonal variations of seismic velocities Merapi volcano, Indonesia, *Geophys. Res. Lett.*, **33**(21).

Shapiro, N. M. and M. Campillo, (2004). Emergence of broadband Rayleigh waves from correlations of ambient seismic noise, *Geophys. Res. Lett*. **31**, L07614, doi: 10.1029/2004GL019491.

Shapiro, N. M., M. Campillo, L. Stehly, and M. H. Ritzwoller, (2005). High resolution surface-wave tomography from ambient seismic noise, *Science* **307** (5715), 1615– 1618.

Snieder, R., (2004). Extracting the Green's function from the correlation of coda waves: A derivation based on stationary phase, *Physical Review*, 69.

Snieder, R., (2006). The theory of Coda Wave Interferometry, *Pure Appl. Geophys*., **163**, 455–473.

Snieder, R., A. Gret, H. Douma, and J. Scales, (2002). Coda Wave Interferometry for estimating nonlinear behavior in seismic velocity, *Science*, 295, 2253–2255.

Snieder R. and E. Safak, (2006). Extracting the building response using seismic interferometry; theory and application to the Millikan Library in Pasadena, *California. Bull. Seism. Soc. Am*. **96**, 586–598.

Şaroğlu F., Ö. Emre, I. Kuşçu, (1992). Active fault map of Turkey, Publ. Miner. Res. Explor. Ins. Turkey, Ankara, Turkey.

Şengör A.M.C., (1979). The North Anatolian transform fault: its age, offset and tectonic significance, *J. Geol. Soc. Lond*., **136**, 269–282.

Şengör, A.M.C. and Yılmaz, Y., (1981). Tethyan evolution of Turkey: a plate tectonic approach, *Tectonophysics*, **75**, 181-241.

Şengör, A.M.C., S., Ozeren, T., Genc and E., Zor, (2003). East Anatolian high plateau as a mantle-supported, north-south shortened domal structure, *Geophys. Res. Lett*., **30**(24), 8045, doi:10.1029/2003GL017858

Stehly, J., M., Campillo, B., Fromenta nd R.L., Weaver, (2008). Reconstructing Green's function by correlation of the coda of the correlation (C^3) of ambient noise, *Journal of Geophysical Research*, **113**, B11306.

Stein, R.S., Barka, A. and J. H. Dieterich, (1997). Progressive failure of the North Anatolian fault since 1939 by earthquake stress triggering, *Geophys. J. Int.,* **128**, 594-604.

Tibi, R., Bock, G., Xia, Y., Baumbach, M., Grosser, H., Milkereit, C., Karakisa, S., Zünbül, S., Kind, R. and J. Zschau, (2001). Rupture processes of the 1999 August 17 Izmit and November 12 Düzce (Turkey) earthquakes, *Geophys. J. Int.,* **144**, F1-F7.

Toksöz, M., C. Cheng, and A. Timur, (1976). Velocities od Seismic Waves in Porous Rocks, *Geophy.*, **41**(4), 621–645. doi: 10.1190/1.1440639

Toksöz, M.N. and R.T. Lacoss, (1968). Microseisms: mode structure and sources, *Science*, 159:872–3.

Toksöz M.N., Shakal, A.F. and A. J. Michael, (1979). Space-time migration of earthquakes along the North Anatolian Fault and seismic gaps, *PAGEOPH,* **117**, 1258-1270.

Trampert J. and J.H. Woodhouse, (2007). Global phase velocity maps of Love and Rayleigh waves between 40 and 150 seconds, *Geophys. J. Int*., **122**, 675-690.

Tunç B., D. Caka, T.S. Irmak, H. Woith, S. Tunç , S. Barış, M.F. Özer, B.G. Lühr, E. Günther, H. Grosser and J. Zschau ,(2011). The Armutlu Network: an investigation into the seismotectonic setting of Armutlu-Yalova-Gemlik and the surrounding regions, *Annals of Geophys*., **54** (1), doi: 10.4401/ag-4877

Türkelli, N., E. Sandvol, E. Zor, R. Gök, T. Bekler, A. Al-Lazki, H. Karabulut, S. Kuleli, T. Eken, C. Gürbüz, S. Bayraktutan, D. Seber, and M. Barazangi, (2003). Seismogenic Zones in Eastern Turkey, *Geophys. Res. Lett.,* **30**(24), 8039, *doi:*10.1029/2003GL018023.

Xia, J., R. D. Miller, C. B. Park, and G. Tian, (2003). Inversion of high frequency surface waves with fundamental and higher modes, *Journal of Applied Geophysics*, **52**, 45-57.

Wessel, P., and W. H. F. Smith, (1995). New version of the generic mapping tools released, *Eos Trans. AGU*, **76** (33), 329, doi:10.1029/95EO00198

Vanacore, E. A., T. Taymaz, and E. Saygin, (2013). Moho structure of the Anatolian Plate from receiver function analysis, *Geophys. J. Int*. **193**, no. 1, 329–337, doi: 10.1093/gji/ggs1107.

Vidale J. E. and Y-G. Li, (2003). Damage to the shallow Landers fault from the nearby Hector Mine earthquake, *Nature*, **421**, 524-526.

Waldhauser, F. and W.L. Ellsworth, (2000). A double-difference earthquake location algorithm: Method and application to the northern Hayward fault, California, *Bull. Seismol. Soc. Am.*, **90**, 1353–1368

Wapenaar, K., (2003). Synthesis of an inhomogeneous medium from its acoustic transmission response, *Geophysics*, 68-1756-1759.

Wapenaar, K., (2004). Retrieving the elastodynamic Green's function of an arbitrary inhomogeneous medium by cross correlation, *Phys. Rev. Lett*. **93**, 254301.

Wapenaar, K. and J., Fokkema, (2006). Green's function representations for seismic interferometry. *Geophysics*, (**71**), S133–S144.

Warren, L.M., S.L. Beck, C.B. Biryol, G. Zandt, A.A. Özacar and Y. Yang, (2013). Crustal velocity structure of central and eastern Turkey from ambient noise tomography, *Geophys. J. Int*., doi: 10.1093/gji/ggt210

Weaver, R. L. and O. I. Lobkis, (2001), Ultrasonics without a source: Thermal fluctuation correlations at MHz frequencies, *Phys. Rev. Lett*. **87**, 134301.

Weaver, R. L., and O. I. Lobkis, (2004). Diffuse waves in open systems and the emergence of the Green's function, *J. Acoust. Soc. Am*., **116**(5), 2731–2734, doi:10.1121/1.1810232.

Weaver, R. L., (2005). Information from seismic noise, *Science*, **307***,* 5715*,* 1568–1569.

Wegler, U., B.-G. Luhr, R. Snieder, and A. Ratdomopurbo, (2006). Increase of shear wave velocity before the 1998 eruption of Merapi volcano (Indonesia), *Geophys. Res. Lett.*, **33**, L09303, doi:10.1029/2006GL025928.

Wegler, U., and C. Sens-Schönfelder, (2007). Fault zone monitoring with Passive Image Interferometry, *Geophys. J. Int*., **168**, 1029–1033, doi:10.1111/j.1365-246X.2006.03284.x.

Wegler, U., H. Nakahara, C. Sens-Schönfelder, M. Korn, and K. Shiomi, (2009). Sudden drop of seismic velocity after the 2004 M_w 6.6 mid-Niigata earthquake, Japan, observed with Passive Image Interferometry, *J. Geophys. Res*., **114**(B06305), 1–11.

Whitcomb, J.H., Garmany, J.E. and Anderson, D.L., (1973). Earthquake prediction: variation of seismic velocities before the San Francisco earthquake, *Science,* **180**, 632–635.

Wright, T., E. Fielding and B. Parsons, (2001). Triggered slip: observations of the 17 August 1999 Izmit (Turkey) earthquake using radar interferometry, *Geophys. Res. Lett.*, **28**(6), 1079-1082.

Yang, Y., M. H. Ritzwoller, A. L. Levshin, and N. M. Shapiro, (2007). Ambient noise Rayleigh wave tomography across Europe, *Geophys. J. Int*., **168**, 259–274, doi:10.1111/j.1365-246X.2006.03203.x.

Yang, Y. and M. H. Ritzwoller, (2008). Characteristics of ambient seismic noise as a source for surface wave tomography, *Geochem. Geophys. Geosyst.,* 9, Q02008, doi:10.1029/2007GC001814.

Yao, H., van der Hilst, R., and M. de Hoop, (2006). Surface-wave array tomography in SE Tibet from ambient seismic noise and two-station analysis – I. Phase velocity maps, *Geophysical Journal International*, **166**, 732–744.

Yu, W., T.-R. A. Song and P.G. Silver, (2013). Temporal velocity changes in the crust associated with the great Sumatra earthquakes, *Bull. of Seism. Soc of Am*., **103**(5), 2797-2809.

Zaccarelli, L., N.M. Shapiro, L. Faenza, G. Soldati and A. Michelini, (2011). Variations of crustal elastic properties during the 2009 L'Aquila earthquake inferred from cross-correlations of ambient seismic noise, Geophys. Res. Lett., 38(24), doi: 10.1029/2011GL049750.

Zhao, P., and Z. G. Peng, (2009). Depth extent of damage zones around the central Calaveras fault from waveform analysis of repeating earthquakes, *Geophys. J. Int*., **179**, 1817–1830, doi: 10.1111/j.1365-246X.2009.04385.x.

Zheng, X., Jiao, W., Zhang, C., and L., Wang, (2010). Short-period Rayleigh-wave group velocity tomography through ambient noise cross-correlation in Xinjiang, Northwest China. *Bulletin of the Seismological Society of America*, **100**, 1350–1355.

Zor, E., E. Sandvol, C. Gürbüz, N. Türkelli, D. Seber and M. Barazangi, (2003). The crustal structure of the east Anatolian plateau (Turkey) from receiver functions, *Geophys. Res. Lett*., 30(24).

Zor, E., S. Özalaybey and C. Gürbüz, (2006). The crustal structure of the eastern Marmara region, Turkey by teleseismic receiver functions, *Geophys, J. Int*., **167**, 213-222.

Curriculum vitae

Curriculum vitae was removed from the electronic version.

List of Figures

Page

Chapter 2 – Theoretical background

Chapter 3 – Tectonic setting

Chapter 4 - Ambient noise analysis in the eastern Sea of Marmara region in NW Turkey: Lateral variations of the crustal velocity field

Chapter 5 - Coseismic velocity change associated with the 2011 Van earthquake (M7.1): Crustal response to a major event

Acknowledgements

I would like to thank to my supervisor Prof. Dr. Marco Bohnhoff for giving me a chance to work within his group and further supporting my interest in studying ambient seismic noise. There are not enough words to express my gratitude to Dr. Fatih Bulut for his help, support and confidence in me during this study. This work would not be possible without their guidance.

I would like to thank to Dr. Christoph Sens-Schönfelder for his valuable comments and time he spared for discussion. I would like to extend my thanks to Prof. Dr. Argun Kocaoğlu and Prof. Dr. Abdullah Karaman for their support and encouragement since the very beginning of my long journey in geophysics. The last but not the least, Prof. Dr. Valerie Maupin, maybe not within the time frame of this study but I learnt a lot from her about surface waves, scattering and many more.

Thanks to my dear office mate, neighbor and friend Patrizia Martinez-Garzon☺. She, Elma and Masline made my life easier and happier in Potsdam. Thanks to all my PhD colleagues and everyone in Section 3.2 Geomechanics and Rheology. Dear Rita Hamlischer, you are an angel. Thanks also to Tuna Eken, for his support and friendship.

And thanks to the unprecedented love and support of my family: Nadire –canım annem- ve E. Merve – canım kardeşim–, her zaman yanımda olduğunuz için teşekkür ederim.

Balım. Yolumu aydınlattın. Teşekkür ederim.